Doctoral Dissertation

Studies on Correlation between Charge Carrier Mobility and Backbone Configuration of Conductive Polymers

Takahiro Fukumatsu

January 2015

Division of Applied Chemistry

Graduate School of Engineering

Osaka University

Doctoral Dissertation

Studies on Correlation between Charge Carrier Mobility and Backbone Configuration of Conductive Polymers

（導電性高分子の骨格構造と
電荷移動度の相関に関する研究）

Takahiro Fukumatsu

January 2015

Division of Applied Chemistry

Graduate School of Engineering

Osaka University

Preface

The present dissertation is the collection of studies that have been performed between 2010 and 2015 under direction of Professor Shuhei Seki at Division of Applied Chemistry, Graduate School of Engineering, Osaka University. The studies in this thesis are concerned with the correlation between the charge carrier mobility and backbone structure of conjugated polymers.

Takahiro Fukumatsu

Seki Laboratory
Division of Applied Chemistry
Graduate School of Engineering
Osaka University

January 2015

Contents

General Introduction

1. Background

In recent years, conjugated polymers have attracted much interest as alternative materials for inorganic semiconductor, and they have been indispensable elements for organic electronic devices, such as organic photovoltaic cells (OPV),[1] organic field-effect transistors (OFET),[2] and organic light emitting diodes (OLED).[3] In electronic devices, charge carrier mobility is one of the most important factor. Although a lot of conjugated polymers were synthesized for high charge carrier mobility, the value is at most 0.1 – 1 $cm^2\ V^{-1}\ s^{-1}$ order,[4] which is much lower than inorganic semiconductors. Therefore, organic semiconductors with high charge carrier mobility are desired as a key to success for development of organic electronic devices.

Improvement of charge transport property in conjugated polymer can be attained not only by producing a new material but also by controlling polymer structure. Persistence length q represents a basic property quantifying the stiffness of a polymer in worm-like chain model.[5] Meanwhile, linear structure of polymer backbone may be advantage for their charge transport property because the conductive property of conjugated polymer arises from the extension of π-conjugated plane along main chain. For example, polyfluorene showed the charge carrier mobility of 0.7 $cm^2V^{-1}\ s^{-1}$ with long persistence length q = 8.5 nm.[6] Furthermore, poly[2-methoxy-5-(2-ethylhexyloxy)-1,4-phenylenevinylene] (MEH-PPV) with 6.0 nm persistence length shows good charge carrier mobility of 0.46 $cm^2\ V^{-1}\ s^{-1}$. [7] Therefore, persistence length can be a good index for charge transport properties, and it is of great worth to investigate the correlation.

In order to evaluate intramolecular charge carrier mobility of conjugated polymer whose

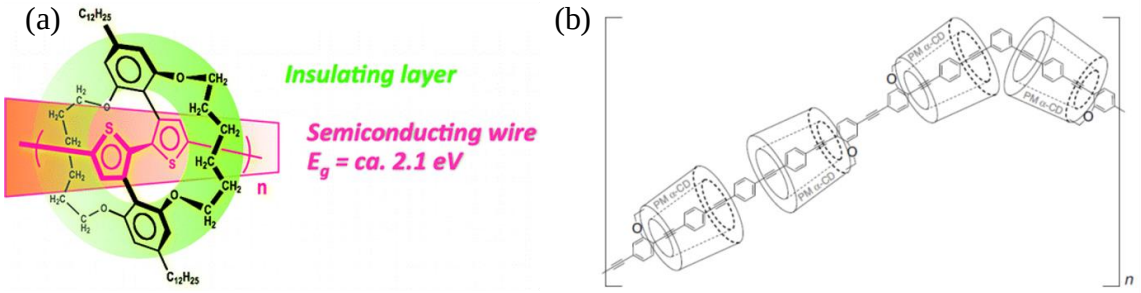

Figure 1. Conjugated polymers for evaluating the intramolecular charge carrier mobility by covering main chain by (a) side chain[8] and (b) rotaxane structure. [9F]

chain structure is regulated, covering polymer main chain is one of the efficient methods to exclude the effect of intermolecular charge transport (Figure 1). Sugiyasu et al. have reported that the intramolecular charge carrier mobility of self-threading polythiophene covered by own side alkyl chains was evaluated to be 0.9 cm^2 V^{-1} s^{-1}.[8] Moreover, Terao et al. have utilized rotaxane structure to wrap up a poly(phenyleneethynylene) chain and showed the intramolecular charge carrier mobility of 8.5 cm^2 V^{-1} s^{-1}, which is very high as an organic material.[9] This technique is good for determining the correlation between intramolecular charge carrier mobility and polymer configuration.

To attain facile control of secondary structure, polymer alloy could be a hopeful candidate. Polymer alloys have been used since 1940's to increase the impact resistance, heat resistance, chemical resistance, and so on.[10] As typical polymer alloy materials, there are ABS resin (Acrylonitrile-Butadiene-Styrene copolymer resin) and polycarbonate/ABS resin, and these polymer alloy have been used everywhere. The reason why polymer alloy technique is actively investigated is due to their facile modulation. By the kind of polymers, blend ratio, and temperature, the phase structure of polymer alloy is changed. Phase structure formed by polymer alloy is classified into three phases; i.e. stable, semistable and unstable phases. Interestingly, in semistable state, although phase segregation occurs via nucleation-growth process, polymer configuration

can be retained at room temperature because phase segregation speed was very low. By utilizing this property, high impact polystyrene (HIPS), polystyrene/butadiene rubber polymer alloy have been used.

In order to evaluate charge carrier mobility of conjugated polymer whose backbone structure is confined by polymer alloy technique, the conductivity measurement by direct current (DC) methods such as FET or time-of-flight (TOF) measurement seems to be difficult, because the charge transport property evaluated by these methods can be affected not only by backbone structure but also external factors such as impurity, electrode contact, and so on. (Figure 2a). As a measurement replacing these DC methods, flash-photolysis time-resolved microwave conductivity measurement (FP-TRMC) is an efficient methods (Figure 2b).[11] In FP-TRMC measurement, charge carrier is injected by pulse-laser, and microwave is used as a probe of charge motion, so that, charge transport property in a few nano-meter can be evaluated. Therefore, non-electrode charge carrier mobility measurement without influence of charge trap sites such as impurity and crystal boundary can be achieved by FP-TRMC.

The following sections described the fundamental knowledge of FP-TRMC measurement, statistical polymer configurations, and polymer alloys.

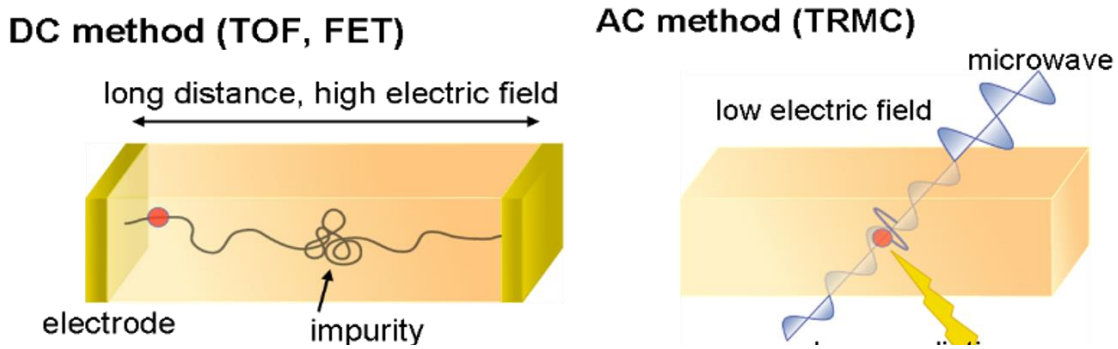

Figure 2. Schematics of DC and AC measurement.

2. Principal of Flash Photolysis Time-Resolve Microwave Conductivity (FP-TRMC)

In general, dielectric characteristic of material for electromagnetic wave is represented as complex dielectric constant $\varepsilon_r = \varepsilon_r' - i\varepsilon_r''$, where ε_r' and ε_r'' are dielectric constant and dielectric loss, respectively. Here, ε_r'' corresponds to absorption of electromagnetic wave caused by inability to follow to electromagnetic wave oscillation. This absorption occurs by interaction between electromagnetic wave and molecular polarization, ionic polarization, orientation polarization of dipole moment, and charge carrier. In X-band microwave (~9 GHz), microwave electric loss depends on dipole moment and motion of charge carrier. When microwave absorption by charge carrier occurs, the Joule heat is generated proportional to resistance *R*, and conductivity σ is reciprocal number of *R*. Therefore, microwave absorption by charge carrier is closely related to conductivity.

In FP-TRMC, charge injection is performed by radiation of pulse laser, and microwave of small power (~few mW) is used as a probe (Figure 3).[11] The resonance cavity is used to amplify the microwave absorption because the efficiency of charge generation by pulse laser is generally small (~10^{-3} – 10^{-4}). Here, complex conductivity change $\Delta\sigma$ and change of *Q* value in the resonance cavity induced by conductivity change are represented by the following equations;

$$\Delta\sigma = \Delta\sigma' + \Delta\sigma'' \quad (1)$$

$$\Delta\frac{1}{Q} - i\frac{2\Delta\omega_0}{\omega_0^2} = \frac{4\pi}{\omega_0}(\langle\Delta\sigma'\rangle + i\langle\Delta\sigma''\rangle) \quad (2)$$

where $\Delta\sigma'$, $\Delta\sigma''$, and ω_0 are the real part and the imaginary part of conductivity change, and resonance frequency, respectively. From Equation (2), the decrease of microwave power induced by the absorption by charge carriers is correlated with the decrease of *Q*

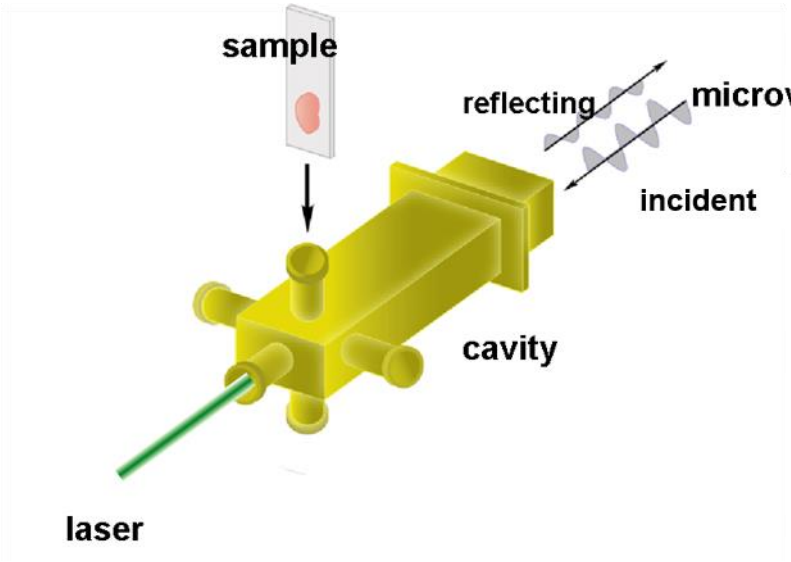

Figure 3. Schematics of FP-TRMC measurement.

value. Therefore, the real part of conductivity $\Delta\sigma'$ is proportional to the dielectric loss $\Delta\varepsilon_r''$.

The change of conductivity evaluated by FP-TRMC technique is proportional to the power of reflected microwave P_r and its variation ΔP_r;

$$\langle \Delta\sigma \rangle = \frac{1}{A}\frac{\Delta P_r}{P_r} \tag{3}$$

$$A = \frac{\pm Q\left(1/\sqrt{R_0} \pm 1\right)}{\pi f_0 \varepsilon_0 \varepsilon_r} \tag{4}$$

where A, f_0, and R_0 are sensitivity factor, resonance frequency, and ratio of incident and reflected microwave power, respectively. Here, carrier generation efficiency ϕ is defined as the probability of the number of charge carrier which is not deactivated within FP-TRMC time resolution (~50 ns) divided by the photon number absorbed by material. Transient conductivity $\phi\Sigma\mu$ is shown in the equation by using ϕ;

$$\phi\Sigma\mu = \frac{1}{e \cdot I_0 \cdot F_{\mathrm{Light}}}\frac{1}{A}\frac{\Delta P_r}{P_r} \tag{5}$$

where F_{Light} is a factor including compensation of special distribution of electric field and charge carrier. $\phi\Sigma\mu$ has the same dimension as charge carrier mobility, and $\Sigma\mu$ is obtained

by evaluating ϕ by another measurement. As the methods to evaluating ϕ, transient absorption spectroscopy (TAS) and contact electrodes methods are available. Thus, by combining FP-TRMC and TAS or contact electrodes methods, charge carrier mobility can be estimated.

3. Polymer Structure and Their Statistical Treatment

Unlike low molecular weight compounds, the shape of polymers cannot be defined uniquely because of their diversity of the chain structure. Therefore, statistical treatment of polymer structure is needed to evaluate the structural characteristics of polymers.[5, 12]

Now, in order to treat average chain dimension statistically, a linear macromolecular chain consisted of n+1 atoms and n bond vectors $\boldsymbol{r}_i$ (i = 1 ~ n) is considered. b, θ, and φ_i are the absolute value of bond vector $\boldsymbol{r}_i$ and the angle between adjacent bond vectors, respectively. The end-to-end distance $\boldsymbol{R}$ and mean-square end-to-end distance $\langle R^2 \rangle$ are represented by the following equation;

$$\boldsymbol{R} = \boldsymbol{r}_1 + \boldsymbol{r}_2 + \cdots \boldsymbol{r}_n = \sum_{i=1}^{n} \boldsymbol{r}_i \tag{6}$$

$$\langle R^2 \rangle = \langle \boldsymbol{R} \cdot \boldsymbol{R} \rangle = nb^2 + 2 \sum_{i=1}^{n-1} \sum_{j=i+1}^{n} \langle \boldsymbol{r}_i \cdot \boldsymbol{r}_j \rangle \tag{7}$$

where $\langle \cdots \rangle$ means the statistical average of all rotational isomeric states. $\langle R^2 \rangle$ is an important factor describing the average chain dimension. Then, the radius of gyration S is defined by $\boldsymbol{S}_i$ vector, which corresponds to the vector from the center of gravity of polymer to n_ith atom. Assuming that mass of atom is constant, S and mean-square radius of gyration $\langle S^2 \rangle$ are shown in following equations;

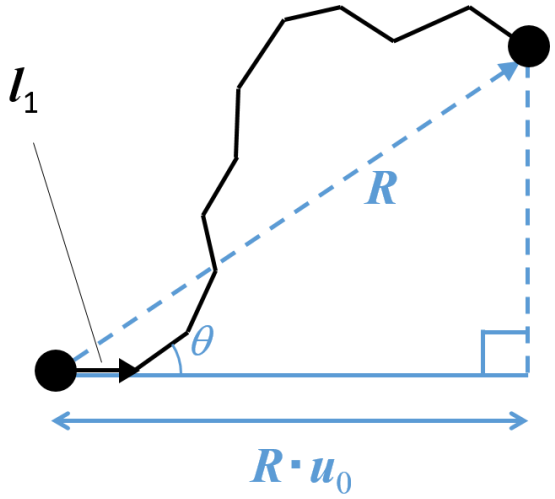

Figure 4. Schematics of worm-like chain

$$S^2 = \frac{n}{n+1}\sum_{i=0}^{n} \boldsymbol{S}_i{}^2 \tag{8}$$

$$\langle S^2 \rangle = \frac{1}{(n+1)^2}\sum_{i=0}^{n-1}\sum_{j=i+1}^{n} \langle R_{ij}^2 \rangle \tag{9}$$

$\langle S^2 \rangle$ is also an important indicator which shows the average chain dimension.

Although this model reflects local structure of a polymer chain, the equation of $\langle R^2 \rangle$ and $\langle S^2 \rangle$ is too much complex to understand intuitively. As the replacement for this model, worm-like chain model is used (Figure 4).[5] In this model, polymer is treated as a freely rotating chain (φ is free) with bond number n, and with constant bond length b and bond angle θ. When the vector $\boldsymbol{u}_0$ defined as the unit vector which is parallel to the bond vector $\boldsymbol{r}_1$, the average of projection length of $\boldsymbol{R}$ along $\boldsymbol{r}_1$ vector $\langle \boldsymbol{R} \cdot \boldsymbol{u}_0 \rangle$ is represented by the follow equation;

$$\langle \boldsymbol{R} \cdot \boldsymbol{u_0} \rangle = b^{-1}\sum_{i=1}^{n} \langle \boldsymbol{r}_1 \cdot \boldsymbol{r}_i \rangle = b\frac{1 - \langle \cos\theta \rangle^n}{1 - \cos\theta} \tag{10}$$

and persistence length q is defined as follow;

$$q = \lim_{n\to\infty} \langle \boldsymbol{R} \cdot \boldsymbol{u}_0 \rangle = \frac{b}{1-\cos\theta} = \frac{\varepsilon}{k_B T} \tag{11}$$

where ε, k_B, and T are bending elastic constant, Boltzmann constant, and temperature, respectively. q describes how polymer can extend toward $\boldsymbol{r}_1$. By combination of Equation (7), (9) and (11), $\langle R^2 \rangle, \langle S^2 \rangle$ are represented by the follow equations;

$$\langle R^2 \rangle = 2qL - 2q^2\left(1\text{-}e^{-L/q}\right) \tag{12}$$

$$\langle S^2 \rangle = \frac{qL}{3} - q^2 + \frac{2q^3}{L} - \frac{2q^4}{L^2}(1 - e^{-L/q}) \tag{13}$$

where L is path length (= nb). By evaluating $\langle S^2 \rangle$ from light scattering measurement or viscosity determination, q can be calculated by this equation.

4. Polymer Alloy Technique

Polymer alloy technique have been used since 1940's. In this chapter, basic physics of phase states of polymer alloy is explained.

In Figure 5, Gibbs free energy change for mixing of two kinds of polymers ΔG_{mix} is represented by the following equations;[13]

$$\Delta G_{mix} = -T\Delta S_{mix} + \Delta H_{mix} \tag{14}$$

$$\frac{\Delta G_{mix}}{RT} = \frac{\phi_A}{N_A}\ln\phi_A + \frac{\phi_B}{N_B}\ln\phi_B + \phi_A\phi_B\chi_{AB} \tag{15}$$

where ΔS_{mix}, ΔH_{mix}, N_A, N_B, ϕ_A, ϕ_B, T, R, and χ are mixing entropy change, mixing enthalpy change, polymerization degree of polymer A and B, volume fraction of polymer A and B, temperature, gas constant, and chi-parameter, respectively. Mixing entropy change ΔS_{mix} in Equation (14) corresponds to the first term and the second term in Equation (15), and mixing enthalpy change ΔH_{mix} is the third term. Equation (15) describes that when N_A, N_B are sufficiently high values, chi-parameter χ should fulfill a

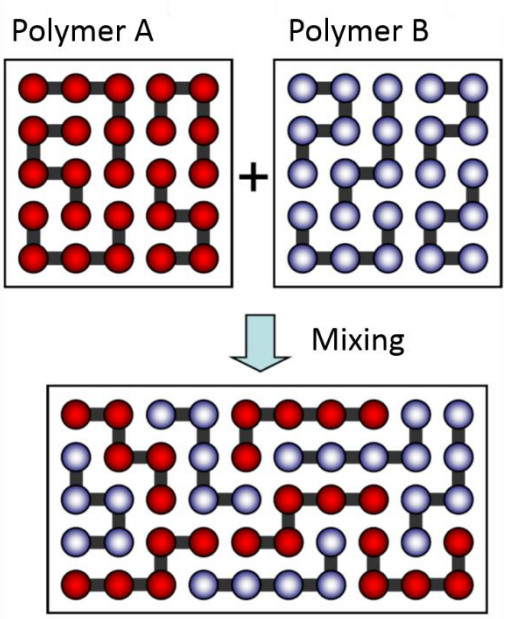

Figure 5. Schematics of mixing of polymers

very small value for homogeneous phase. It is for this reason that phase segregation structure is formed in almost all combinations of polymers. Critical point at which homogeneous phase can be formed by mixture of polymer A and B is represent by the following equation;

$$\frac{\mathrm{d}^3(\Delta G_{\mathrm{mix}}/k_{\mathrm{B}}T)}{\mathrm{d}{\phi_{\mathrm{A}}}^3} = \frac{\mathrm{d}^2(\Delta G_{\mathrm{mix}}/k_{\mathrm{B}}T)}{\mathrm{d}{\phi_{\mathrm{A}}}^2} = 0 \tag{16}$$

Critical chi-parameter χ_{critical} and critical volume fraction of polymer A $\phi_{\mathrm{A,\ critical}}$ are described as follow;

$$\chi_{\mathrm{critical}} = \frac{1}{2}\left(\frac{1}{\sqrt{N_{\mathrm{A}}}} + \frac{1}{\sqrt{N_{\mathrm{B}}}}\right)^2 \tag{17}$$

$$\phi_{\mathrm{A,critical}} = \frac{\sqrt{N_{\mathrm{B}}}}{\sqrt{N_{\mathrm{A}}} + \sqrt{N_{\mathrm{B}}}} \tag{18}$$

Critical chi-parameter χ_{critical} can be a key to the compatibility of a pair of polymers. If $\chi > \chi_{\mathrm{critical}}$ is satisfied at a certain temperature, phase separation occerrs. Meanwhile, if $\chi < \chi_{\mathrm{critical}}$ is satisfied, homogeneous phase is formed.

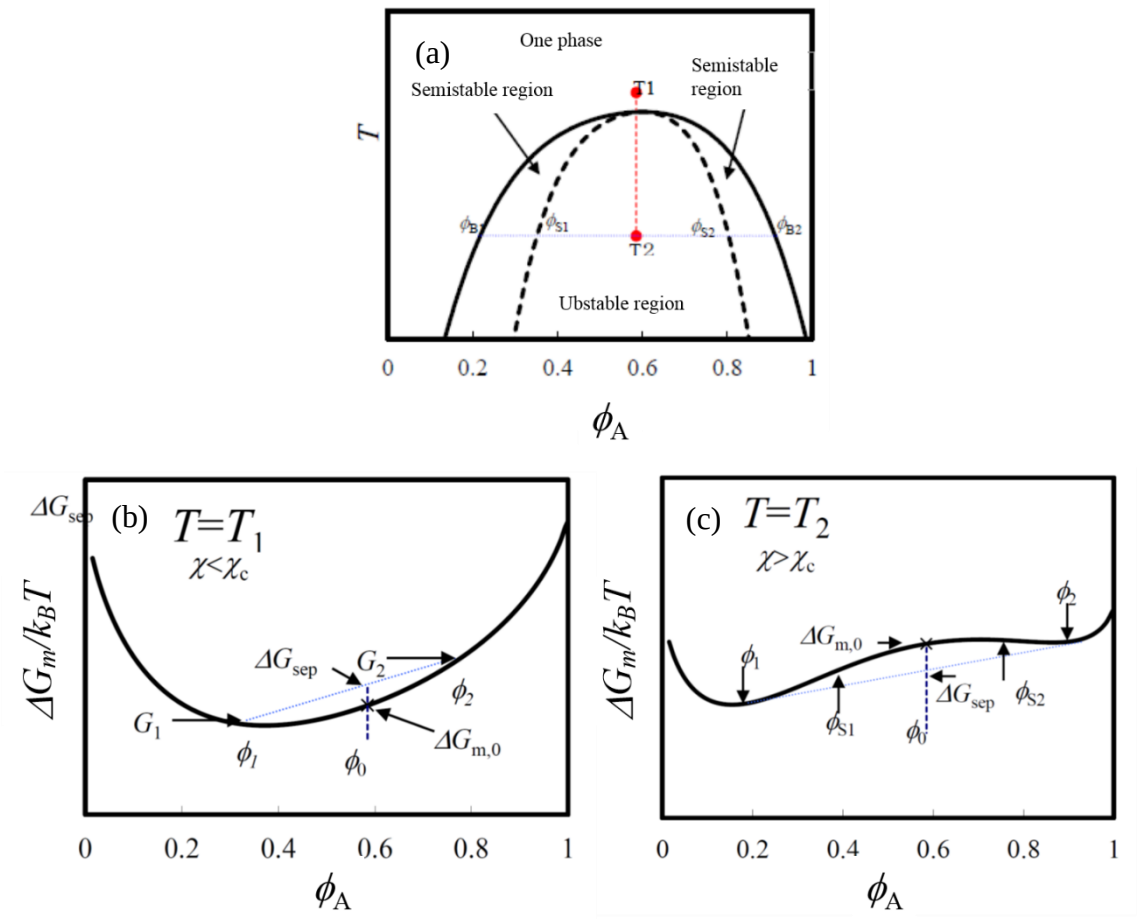

Figure 5. (a) Phase diagram of polymer alloy. Solid line and broken line show binodal line and spinodal line, respectively. (b) (c) Schematic diagrams of free energy curves at (b) $\chi < \chi_{critical}$ and (c) $\chi > \chi_{critical}$ points.

Mixing state of polymer alloy can be changed by temperature and mixing ratio of polymers. Figure 5 shows the phase diagram of polymer alloy and two schematic diagrams of free energy curve. In Figure 5a the vertical axis represents absolute temperature, and the horizontal represents the volume fraction of polymer A. The solid line is the binodal line, which shows the boundary between the one phase and the two phase region. The upper area of binodal line has a homogeneous phase, while phase segregation occurs in the lower area. Figures 5b and 5c show the free energy curves of blend system of polymer A and B at a certain temperature in (b) $\chi < \chi_{critical}$ and (c) χ

$>$ χ_{critical} conoditions. The free energy curve in Figure 5b shows no local manima, and therefore polymers are mixed homogeneously and take mono-phase state. On the other hand, the free energy curve has two local manima in Figure 5c. Let ϕ_1 and ϕ_2 be the volume fractions of polymer A which give minima of free energy change ($\phi_1 < \phi_2$), and the following equation is derived;

$$\left[\frac{\mathrm{d}(\Delta G_{\mathrm{mix}}/k_{\mathrm{B}}T)}{\mathrm{d}\theta}\right]_{\phi=\phi_1} = \left[\frac{\mathrm{d}(\Delta G_{\mathrm{mix}}/k_{\mathrm{B}}T)}{\mathrm{d}\theta}\right]_{\phi=\phi_2} = \frac{\Delta G_{\mathrm{mix}}(\phi_2) - \Delta G_{\mathrm{mix}}(\phi_1)}{\phi_2 - \phi_1} \qquad (19)$$

If $\phi_{\mathrm{A}} < \phi < \phi_{\mathrm{B}}$, the phase segregation proceeds because the mixing Gibbs free energy of mono-phase state at ϕ becomes larger than that of binary phase state at ϕ_1 and ϕ_2.

Taking a closer look about Figure 5c, there are two inflection point at $\phi_1 < \phi < \phi_2$ region. Let $\phi_{\mathrm{r}1}$ and $\phi_{\mathrm{r}2}$, called spinodal point, be the volume fractions at inflection point ($\phi_{\mathrm{r}1} < \phi_{\mathrm{r}2}$), and spinodal line is the line connecting spinodal point. In the $\phi_{\mathrm{r}1} < \phi < \phi_{\mathrm{r}2}$ region, polymer alloy structure becomes binary phase via spinodal decomposition and the continuous phase structure is formed, which is induced by polymer fluctuations. Meanwhile, in $\phi_1 < \phi < \phi_{\mathrm{r}1}$ and $\phi_{\mathrm{r}2} < \phi < \phi_2$ regions, polymer alloy structure becomes binary phase via nucleation-growth process and sea-island structure is formed. In this region, the polymer structure can be retained at room temperature unless external stimuli is given because of the slow diffusion of polymers in polymer alloy. Therefore, the polymer alloy technique can be used as a way to modulate secondary structure.

5. Outline of This work

In this dissertation, the correlation between polymer main chain and charge transport property of polymer was investigated by FP-TRMC measurement.

Chapter 1

The correlation between the intramolecular charge carrier mobility and the secondary structure of fluorene-thiophene copolymers was investigated by FP-TRMC technique. FP-TRMC measurement demonstrated the intramolecular charge transport property of amorphous polymer can be detected in FP-TRMC technique. The intramolecular charge carrier mobilities of fluorene-thiophene copolymers showed odd-even effect for the backbone structure. It was suggested that charge transport property along the main chain reflected the secondary structure of polymer backbone.

Chapter 2

The intramolecular charge carrier mobility of triphenylamine (TPA)–fluorene copolymers and the influence of TPA unit on their charge transport property were investigated by FP-TRMC measurement. It is demonstrated the charge carrier mobility of FP-TRMC strongly reflected the intramolecular charge transport property rather than SCLC and FET ones. Moreover, it was elucidated that intramolecular charge carrier mobility estimated by FP-TRMC measurement reflected not only the distribution of the singly-occupied molecular orbital (SOMO) but also the secondary structure of polymer backbone.

Chapter 3

Polymer alloys of regio-regular poly(3-hexylthiophene-2,5-diyl) (P3HT) and polystyrene (PS) matrix were investigated by FP-TRMC and steady-state photoabsorption spectroscopy, respectively. FP-TRMC measurement were demonstrated

that in low P3HT concentration film the contribution of *inter*-molecular charge carrier mobility is half of the pristine one. It was suggested that the information about the minimum one-dimensional *intra*-molecular mobility of 0.18 cm^2/Vs was evaluated.

6. References and Notes

[1] Facchetti, A. *Chem. Mater.* **2011**, *23*, 733.

[2] (a) Horowitz, G. *Adv. Mater.* **1998**, *10*, 365. (b) Wang, C.; Dong, H.; Hu, W.; Liu, Y. Zhu, D. *Chem. Rev.* **2012**, *112*, 2208.

[3] Kulkarni, A.P.; Tonzola, C.J.; Babel, A.; Jenekhe, S.A. *Chem. Mater.* **2004**, *16*, 4556.

[4] Sirringhaus, H. *Adv. Mater.* **2014**, *26*, 1319.

[5] (a) Kratky, O.; Porod, G. *Recl. Trav. Chim.* **1949**, *68*, 1106. (b) Doi, M.; Edwards, S. F. In *The Theory of Polymer Dynamics*, Clarendon Press, Oxford, 1990. (c) Rubinstein, M.; Colby, R. H. In *Polymer Physics*, Oxford University Press, Oxford, 2003.

[6] (a) Lyons, B. P.; Monkman, A. P. *Phys. Rev. B* **2005**, *71*, 235201. (b) Shibano, Y.; Imahori, H.; Sreearunothai, P.; Cook, A. R.; Miller, J. R. *J. Phys. Chem. Lett.* **2010**, *1*, 1492.

[7] (a) Gettinger, C. L.; Heeger, A. J.; Drake, J. M.; Pine, D. J. *J. Chem .Phys.* **1994**, *101*, 1673. (b) Grozema, F. C.; Hoofman, R. J. O. M.; Candeias, L. P.; De Haas, M. P.; Warman, J. M., Siebbeles, L. D. A. *J. Phys. Chem. A* **2003**, *107*, 5976.

[8] Sugiyasu, K.; Honsho, Y.; Harrison, R. M.; Sato, A.; Yasuda, T.; Seki, S.; Takeuchi, M. *J. Am. Chem. Soc*. **2010**, *132*, 14754.

[9] Terao, J.; Wadahama, A.; Matono, A.; Tada, T.; Watanabe, S.; Seki, S.; Fujihara, T.; Tsuji, Y. *Nature Commun.* **2013**, *4*, 1691.

[10] Strobl, G. R. In *The Physics of Polymers Concepts for Understanding Their Structures and Behavior*, Springer-Verlag, New York, 1996.

[11] (a) Warman, J. M.; Piris, J.; Pisula, W.; Kastler, M; Wasserfallen, D.; Müllen, K. *J.*

Am. Chem. Soc. **2005**, *127*, 14257. (b) P. Prins, F. C.; Grozema, J. M. ; Schins, S. ; Patil, U. ; Scherf, L. D. A. ; Siebbeles, *Phys. Rev. Lett.* **2006**, *96*, 146601.

[12] Yamakawa, H.; Fujii, M. *Macromolecules* **1974**, *7*. 128.

[13] (a) Flory, P. J. In *Principles of Polymer Chemistry*, Cornell University Press, New York, 1971. (b) Huggins, M. L. *J. Am. Chem. Soc.* **1942**, *64*, 1712.

Chapter 1

Intramolecular Charge Carrier Mobility in Fluorene-Thiophene Copolymer Films Studied by Microwave Conductivity

1. 1. Abstract

The charge carrier mobility along a molecular wire of fluorene-thiophene copolymers represented by poly-(9,9'-di-n-octylfluorene-co-bithiophene): F8T2 was investigated by flash-photolysis time-resolved microwave conductivity. Moreover, the impacts of the number of oligothiophene units, their composition ratios, and molecular weights was systematically examined. It is revealed that the odd-even number of oligothiophene units has a significant effect on the mobility if they are incorporated into the polyfluorene backbone in high ratio. The structural dependence study and the observed high intramolecular mobility of about 1 cm^2 V^{-1} s^{-1} could be helpful for the design of novel multicomponent conjugated copolymers and its application in organic electronic devices.

1. 2. Introduction

Conjugated polymers have attracted keen attention in recent years due to their potential for low cost, bendable, and large-area via roll-to-roll process organic electronic devices.[1] Multi-component conjugated polymers consisting of donor-acceptor or push-pull type moieties are highly promising materials as color tunable emitting layers in organic light emitting diodes (OLED) and bulk heterojunction frameworks with low-band gap for organic photovoltaic cells (OPV).[2] Therefore, considerable efforts have been devoted to the development of novel copolymers possessing unique electronic and optical properties. Polyfluorene and its copolymers form an integral part of OLED, as they have high absorption coefficient, photoluminescence yield, chemical stability and also due to highly pure blue emission.[3-9] Moreover, their optical properties such as absorption, emission, band gap, the highest occupied molecular orbital (HOMO), and the lowest unoccupied molecular orbital (LUMO) can be easily tuned by the incorporation of appropriate conjugated units into the backbone.

Because of their color tuning property in accordance with the π-conjugation length, fluorene-thiophene (F-T) copolymers have intrigued scientists over a decade. The change of absorption and emission spectra in an F-T amphiphilic block copolymer with the solvent polarity has been demonstrated.[10] The application to OPV is emerging as one of the most imperative topics for F-T copolymers.[11] The most widely known F-T copolymer is poly(9,9'-dioctylfluorene-co-bithiophene), usually abbreviated as F8T2.[12-14] It exhibits a thermotropic and nematic liquid-crystalline behavior above 265 ^{o}C, along with relatively high hole mobility (0.02 cm^2 V^{-1} s^{-1}). Although optical and electronic property of F8T2 are well-documented, some aspects of those copolymers and also similar other multiple-component π-conjugated semiconducting polymers such as the

intrinsic charge transport property along a molecular wire still remain to be addressed.

In the present work, intramolecular charge transport of fluorene-thiophene copolymers was investigated by electrode-less flash-photolysis time-resolved microwave conductivity (FP-TRMC) technique.[15-17] It measures the nanometer-scale mobility of charge carriers under an oscillating microwave electric field. In the amorphous films state, the maximum mobility before deactivation by trapping along the conjugation length was selectively probed. A systematic investigation on the electronic properties of copolymers were performed, in which the number of thiophene units and its composition ratio were changed in order to elucidate the role of oligothiophene units in the charge transport along the polymer backbone.

1. 3. Experimental Section

General Procedure of Polymerization

Unless otherwise noted, reagents and solvents were used as received from Aldrich and Wako Chemical, respectively. fluorene-thiophene copolymers is abbreviated to pFTn-x%, where "n" represents the number of thiophene units which varies from 0 to 4 and x% represents the composition ratio of oligothiophene units.Scheme 1 shows the general procedure of polycondensation. 9,9-di-n-octylfluorene-2,7-diboronic acid bis(1,3-propanediol) ester [0.2 mmol], 2,7-dibromo 9,9-dioctylfluorene [0.2 × (0.5-x) mmol], 2,5-dibromo thiophene oligomer [0.2 × x mmol], $Pd(PPh_3)_4$ [0.02 mmol, Tokyo Chemical Industry Corp.], 5 mL of 2 M K_2CO_3 aqueous solution, Aliquat336 [0.12 mmol] and toluene, 10 mL, were placed in a 50mL flask. Note that x represents the ratio of thiophene unit, for example x is 0.02 for pFTn-2%. The reaction solution was vigorously

Scheme 1. Polymerization of fluorene-thiophene copolymers: pFTn-x%. R_1 : n-octyl. R_2 : H for pFT1, pFT2, and pFT3. In the case of pFT4, R_2 = H and R_3 = n-hexyl for n = 1; R_2, R_3 = H for n = 2-3; and R_2 = n-hexyl, R_3 = H for n = 4.

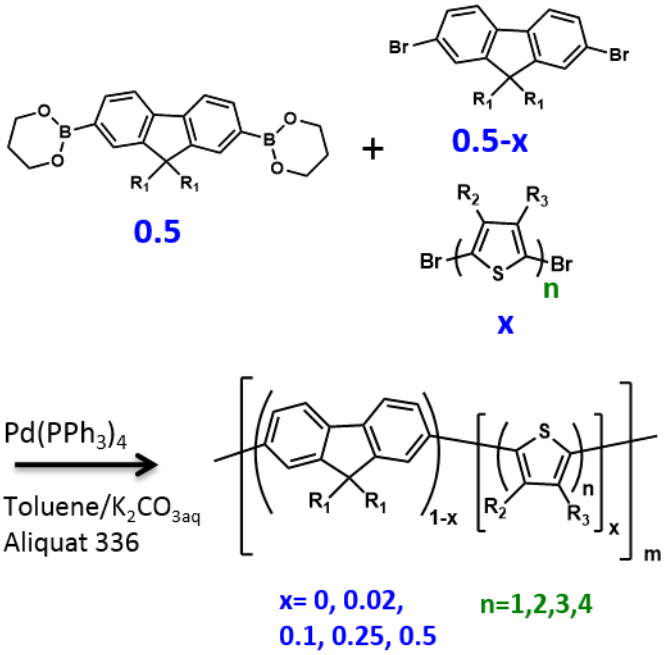

degassed by the freeze-pump-thaw method before polymerization was started. The mixture was heated at 85 ^{o}C for 12-24 h. In the case to obtain low-molecular weight polymers, the polymerization was stopped at an appropriate time. The reaction mixture was poured into methanol. The precipitate was collected and then extracted by toluene with ammonia solution, 1 N HCl_{aq}, and water. The combined organic extract was dried over anhydrous $MgSO_4$, and filtered off from an insoluble fraction. The polymer solution was subjected to Celite chromatography and stirred for 24 h with Pd scavenger. The polymer was precipitated again in methanol.

5,5’’’-Dibromo-3,3’’’-dihexyl-2,2’:5’,2’’:5’’,2’’’-quaterthiophene

Except for quarterthiophene, dibromo-oligothiophenes are commercially available and were used as received. To a N,N’-dimethylformamide solution (10 mL) of 3,3’’’-dihexyl-2,2’:5’,2’’:5’’,2’’’-quaterthiophene (2 mmol) was portionwise added N-

bromosuccinimide (NBS, 4.5 mmol) at -20 °C under argon, and the mixture was allowed to warm to 60 °C. After 20 h of stirring, the reaction mixture was poured into an aqueous solution of KOH (10%, 100 mL) and extracted with toluene. The combined organic extract was washed with water, dried over anhydrous $MgSO_4$, and filtered off from an insoluble fraction. The filtrate was evaporated to dryness under a reduced pressure, and the residue was subjected to column chromatography (SiO_2, AcOEt/hexane 7/3 v/v), to allow isolation of dibromo-quarterthiophene as yelloworange powder in 80% yield. ^{1}H NMR (270 MHz, $CDCl_3$): δ (ppm) 7.10 (d, J = 2 Hz, 2H), 7.00 (d, J = 2 Hz, 2H), 6.90 (s, 2H), 2.71 (t, J = 8 Hz, 4H), 1.61 (t, J = 8 Hz, 4H), 1.32 (m, 12H), 0.89 (t, J = 7 Hz, 6H). FAB-mass: calcd for $C_{28}H_{32}Br_2S_4$, 656.62; found, 656.04.

F8 Polymer: Poly(9,9'-di-n-octylfluorenyl-2,7-diyl)

White powders were obtained in 20-50% yield depending on molecular weight. ^{1}H NMR (270 MHz, $CDCl_3$): *d* (ppm) 7.97-7.77 (br), 7.76-7.63 (br), 2.30-1.85 (br), 1.59-1.47 (br), 1.33-0.98 (br). Anal. Calcd for $(C_{29}H_{40})$n: C, 89.63; H, 10.37. Found: C, 88.83; H, 11.17. Weight-averaged molecular weights (M_w) and polydispersity index (PDI) were 2.0 $\times$ 10^4 (2.0), 5.7 $\times$ 10^4 (2.4), 6.7 $\times$ 10^4 (3.1), 8.3 $\times$ 10^4 (3.7), 15 $\times$ 10^4 (3.8), and 16 $\times$ 10^4 (3.6) g/mol.

pFT1-x% Polymer: Poly(9,9'-di-n-octylfluorene-co-thiophene)

Yellow-green clay (pFT1-2%, yield 48%), yellow-green powder (pFT1-10%, yield 51%), yellow-green powder (pFT1-25%, yield 43%), and red clay (pFT1-50%, yield 22%) were obtained. ^{1}H NMR (270 MHz, $CDCl_3$): δ (ppm) pFT1-2%, 7.99-7.47 (br), 2.37-1.80 (br), 1.59-1.47 (br), 1.33-0.99 (br), 0.99-0.69 (br); pFT1-10%, 7.96-7.47 (br), 2.26-1.94 (br), 1.59-1.47 (br), 1.30-1.05 (br), 0.92-0.73 (br); pFT1-25%, 7.95-7.32 (br), 2.29-1.94 (br), 1.59-1.47 (br), 1.36-1.00 (br), 0.97-0.60 (br); pFT1-50%, 7.93-7.34 (br),

2.21-1.92 (br), 1.59-1.47 (br), 1.30-0.87 (br), 0.87-0.62 (br). Anal. Calcd for pFT1-2%: C, 89.49; H, 10.34; S, 0.16. Found: C, 89.69; H, 10.24; S, 0.07. Anal. Calcd for pFT1-10%: C, 88.98; H, 10.21; S, 0.81. Found: C, 88.38; H, 10.04; S, 1.58. Anal. Calcd for pFT1-25%: C, 88.06; H, 9.98; S, 1.96. Found: C, 87.33; H, 9.66; S, 3.00. Anal. Calcd for pFT1-50%: C, 84.20; H, 8.99; S, 6.81. Found: C, 82.01; H, 10.15; S, 7.84. The molecular ratios of thiophene unit calculated from the elementary analysis were 0.9% for pFT1-2%, 16.6% for pFT1-10%, 28.4% for pFT1-25%, and 52.7% for pFT1-50%. M_w (PDI) of pFT1-2%, pFT1-10%, pFT1-25%, and pFT1-50% were 4.1 $\times$ 10^4 (2.1), 6.6 $\times$ 10^4 (2.0), 3.6 $\times$ 10^4 (1.8), and 5.0 $\times$ 10^3 (1.2) g/mol, respectively.

pFT2-x% Polymer: Poly(9,9'-di-n-octylfluorene-cobithiophene)

Green clay (pFT2-2%, yield 33%), yellow-green powder (pFT2-10%, yield 25%), bright yellow powder (pFT2-25%, yield 48%), and orange powder (pFT2-50%, yield 30-50%, depending on the molecular weight) were obtained. ^{1}H NMR (270 MHz, $CDCl_3$): δ(ppm) pFT2-2%, 7.96-7.41 (br), 2.32-1.87 (br), 1.59-1.47 (br), 1.33-0.98 (br), 0.93-0.68 (br); pFT2-10%, 7.89-7.41 (br), 2.22-1.96 (br), 1.59-1.47 (br), 1.22-1.02 (br), 0.92-0.70 (br); pFT2-25%, 7.93-7.30 (br), 2.29-1.89 (br), 1.59-1.47 (br), 1.26-0.97 (br), 0.97-0.72 (br); pFT2-50%, 7.84-7.01 (br), 2.22-1.88 (br), 1.59-1.47 (br), 1.29-0.94 (br), 0.88-0.65 (br). Anal. Calcd for pFT2-2%: C, 89.36; H, 10.31; S, 0.33. Found: C, 89.49; H, 10.13; S, 0.38. Anal. Calcd for pFT2-10%: C, 88.36; H, 10.05; S, 1.58. Found: C, 88.10; H, 9.84; S, 2.07. Anal. Calcd for pFT2-25%: C, 86.65; H, 9.62; S, 3.73. Found: C, 85.30; H, 9.36; S, 5.34. Anal. Calcd for pFT2-50%: C, 80.38; H, 8.02; S, 11.60. Found: C, 79.41; H, 8.00; S, 12.59. The molecular ratios of thiophene unit calculated from the elementary analysis were 2.3% for pFT2-2%, 11.7% for pFT2-10%, 27.2% for pFT2-25%, and 52.7% for pFT2-50%. M_w (PDI) of pFT2-2%, pFT2-10%, and pFT2-25% were 4.0 $\times$ 10^4 (2.2),

5.3 × 10^4 (2.2), and 4.5 × 10^4 (2.1) g/mol, respectively. M_w (PDI) of pFT2-50% were varied from 6.4 × 10^3 (1.7), 1.2 × 10^4 (1.6), and 4.1 × 10^4 (2.1), to 4.2 × 10^4 (2.1).

pFT3-x% Polymer: Poly(9,9'-di-n-octylfluorene-co-terthiophene)

Yellow-green clay (pFT3-2%, yield 43%), ocher clay (pFT3-10%, yield 36%), bright orange powder (pFT3-25%, yield 47%), and dark red clay (pFT3-50%, yield 15%) were obtained. ^{1}H NMR (270 MHz, $CDCl_3$): δ(ppm) pFT3-2%, 8.02-7.29 (br), 2.36-1.87 (br), 1.59-1.47 (br), 1.32-1.00 (br), 0.94-0.72 (br). pFT3-10%: 8.00-7.12 (br), 2.45-1.83 (br), 1.30-1.00 (br), 0.92-0.70 (br); pFT3-25%, 7.95-7.01 (br), 2.33-1.85 (br), 1.59-1.47 (br), 1.33-0.95 (br), 0.95-0.57 (br); pFT3-50%, 7.73-7.08 (br), 2.13-1.87 (br), 1.59-1.47 (br), 1.32-0.92 (br), 0.92-0.57 (br). Anal. Calcd for pFT3-2%:C, 89.16;H, 10.38; S, 0.45. Found: C, 89.49; H, 10.13; S, 0.38. Anal. Calcd for pFT3-10%: C, 87.77; H, 9.90; S, 2.33. Found: C, 87.62; H, 9.80; S, 2.58. Anal. Calcd for pFT3-25%: C, 85.37; H, 9.29; S, 5.34. Found: C, 85.49; H, 9.31; S, 5.20. Anal. Calcd for pFT3-50%: C, 77.55; H, 7.30; S, 15.15. Found: C, 77.36; H, 7.25; S, 15.39. The molecular ratios of thiophene unit calculated from the elementary analysis were 1.8% for pFT3-2%, 10.1% for pFT3-10%, 19.5%for pFT3-25%, and 50.6% for pFT3-50%.M_w (PDI) of pFT3-2%, pFT3-10%, pFT3-25%, and pFT3-50% were 4.4 × 10^4 (2.1), 7.6 × 10^4 (2.3), 6.5 × 10^4 (2.7), and 7.1 × 10^3 (1.6) g/mol, respectively.

pFT4-x% Polymer: Poly[9,9'-di-n-octylfluorene-co-(3,3'''-dihexyl-2,2':5',2'':5'',2'''-quaterthiophene)].

Dark yellow-green clay (pFT4-2%, yield 38%), yellow powder (pFT4-10%, yield 43%), bright orange powder (pFT4-25%, yield 45%), and red powder (pFT4-50%, yield 53%) were obtained. ^{1}H NMR (270 MHz, $CDCl_3$): δ(ppm) pFT4-2%, 8.03-7.31 (br), 7.22-7.06

(br), 2.93-2.79 (br), 2.38-1.86 (br), 1.82-1.69 (br), 1.60-1.48 (br), 1.42-1.33 (br), 1.32-0.99 (br), 0.95-0.89 (br), 0.88-0.67 (br); pFT4-10%, 7.98-7.38 (br), 7.21-7.00 (br), 2.95-2.68 (br), 2.34-1.83 (br), 1.82-1.67 (br), 1.56-1.43 (br), 1.42-1.32 (br), 1.27-0.97 (br), 0.95-0.89 (br), 0.86-0.57 (br); pFT4-25%, 7.94-7.40 (br), 7.20-7.05 (br), 2.97-2.70 (br), 2.28-1.86 (br), 1.83-1.61 (br), 1.49-1.31 (br), 1.26-0.99 (br), 0.95-0.86 (br), 0.85-0.67 (br); pFT4-50%, 7.77-7.38 (br), 7.21-6.94 (br), 2.95-2.63 (br), 2.15-1.86 (br), 1.84-1.55 (br), 1.53-1.39 (br), 1.39-1.27 (br), 1.25-0.95 (br), 0.95-0.84 (br), 0.85-0.57 (br). Anal. Calcd for pFT4-2%: C, 89.08; H, 10.28; S, 0.64. Found: C, 89.11; H, 10.09; S, 0.80. Anal. Calcd for pFT4-10%: C, 87.14; H, 9.93; S, 2.93. Found: C, 86.90; H, 9.80; S, 3.30. Anal. Calcd for pFT4-25%: C, 84.31; H, 9.43; S, 6.25. Found: C, 83.18; H, 8.90; S, 7.92. Anal. Calcd for pFT4-50%: C, 77.32; H, 8.20; S, 14.49. Found: C, 77.30; H, 8.38; S, 14.31. The molecular ratios of thiophene unit calculated from the elementary analysis were 2.5% for pFT4-2%, 10.3% for pFT4-10%, 26.1% for pFT4-25%, and 49.0% for pFT4-50%. M_w (PDI) of pFT4-2%, pFT4-10%, pFT4-25%, and pFT4-50% were 4.3 $\times$ 10^4 (2.2), 4.8 $\times$ 10^4 (1.9), 7.2 $\times$ 10^4 (2.2), and 6.6 $\times$ 10^4 (2.1) g/mol, respectively.

General Measurements

UV-vis absorption and fluorescence spectroscopies were performed using a JASCO model V-570 and a Hitachi model F-2700 spectrometers, respectively. Polymers were dissolved in spectroscopy-grade chloroform purchased from Wako Chemical Corporation and bubbled by argon gas for at least 10 min. Gel permeation chromatography (GPC) of a Hitachi model (L-2455, L-2130, and L-2350) was performed in tetrahydrofuran (THF) solutions. The molecular weights were calculated using a calibration curve based on polystyrene standards purchased from Aldrich. Nuclear magnetic resonance (NMR) spectroscopy was performed by a JEOL model 270 MHz NMR instrument. Fast atom

bombardment (FAB) mass spectroscopy was performed by a JEOL model JSM-700. Film Preparation. Copolymer films were prepared on a quartz plate by drop-cast from 2 wt % chlorobenzene solutions. The films were dried in a vacuum oven at 60 ^{o}C. Polystyrene (M_w = 2.8 $\times$ 10^5) was purchased from Aldrich. The blend films of pFT4-50% and polystyrene were prepared in the same manner from the mixed chlorobenzene solutions.

Flash-Photolysis Time-Resolved Microwave Conductivity

Transient photoconductivity was measured by flash-photolysis timeresolved microwave conductivity (FP-TRMC).[15-17] A resonant cavity was used to obtain a high degree of sensitivity in the measurement of conductivity. The resonant frequency and the microwave power were set at ~9.1 GHz and 3 mW, respectively, so that the electric field of the microwave was sufficiently small not to disturb the motion of charge carriers. The value of conductivity is converted to the product of the quantum yield: ϕ and the sum of charge carrier mobilities: $\Sigma\mu$, by $\phi\Sigma\mu = \Delta\sigma(eI_0F_{light})^{-1}$, where e, I_0, F_{light}, and $\Delta\sigma$ are the unit charge of a single electron, incident photon density of excitation laser (photons/m^2), a correction (or filling) factor (/m), a transient photoconductivity, respectively. The change of conductivity is equivalent with $\Delta P_r/(AP_r)$,where ΔP_r, P_r, and A area change of reflected microwave power, a power of reflected microwave, and a sensitivity factor [(S/m)$^{-1}$], respectively. Third harmonic generation (THG, 355 nm) of a Nd:YAG laser (Spectra Physics Inc. INDY, 5-8 ns pulse duration) was used as an excitation source. The incident photon density was changed from 0.91 to 9.1 $\times$ 10^{15} photons/cm^2. The data in the text were observed at 9.1 $\times$ 10^{15} photons/cm^2. The sample was set at the highest electric field in a resonant cavity. The experiments were carried out at room temperature.

Flash-Photolysis Transient Absorption Spectroscopy

Transient absorption spectroscopy (TAS) was performed by using third harmonic

generation (THG, 355 nm) of a Nd:YAG laser (Spectra Physics Inc. INDY, 5-8 ns pulse duration) as an excitation and a white light continuum from a Xe lamp as a probe light. The probe light was guided into a wide-dynamic-range streak camera (Hamamatsu C7700) which collects two-dimensional image of the spectrum and time profiles of light intensity. In the solution study, the excitation laser and probe light were aligned by cross-sectional geometry. The solution was bubbled by N_2 for 5 min and loaded in a 1 × 1 cm^2 quartz cell with seal.

Direct Current-Integration

An interdigitated comb-type gold electrode with 5 μm gaps, 40 nm height, and 2 mm width fabricated by lithographic process in the laboratory was used for direct-current (dc) integration experiments.[18] After an appropriate cleaning including UV-ozone treatment, thin polymer film was cast on an electrode by spincoating of chlorobenzene solution of 1 wt % polymer with 1500 rpm for 10 min. Thickness of film was measured by a stylus surface profiler (ULVAC, Dektak 150), giving ca. 50 nm. We confirmed that gaps of interdigitated electrode were filled by polymer from a surface observation. An electrode was placed in a vacuum prober and exposed to the same laser with FP-TRMC experiment. The applied bias was controlled by an Advantest Corp. model R8252 digital electrometer. The transient photocurrent was measured by a Tektronix digital oscilloscope equipped with termination resistance. The applied bias and incident photon density of 355 nm laser were 2 × 10^4 V/cm and 9.1 × 10^{15} photons/cm^2, respectively. The experiments were carried out at room temperature.

Density Functional Theory (DFT)

For the molecular orbital simulations, DFT calculations were performed using the Gaussian03 Rev. E.01 package. The B3LYP and UB3LYP functions with 6-31G(d,p)

basis set were used for neutral and cationic states of pFTn trimers, respectively. The alkyl side chains were replaced by methyl for simplicity.

1. 4. Result and Discussion

1. 4. 1. Synthesis and polymeric properties of pFTn-x% Copolymer

The fluorene-thiophene copolymers were synthesized by a Suzuki-Miyaura coupling. Figure 1 shows the chemical structures of the copolymers: pFTn-x%, where "n" represents the number of thiophene units which varies from 0 to 4 and x% represents the composition ratio of oligothiophene units. For instance, pFT2-50% is identical to poly(9,90-dioctylfluorene-cobithiophene), F8T2, although "8" in the latter abbreviation stands for the carbon number of the side alkyl chain (octyl) at the fluorene unit. The case of n = 0 (or x = 0%) is poly(9,9'-dioctylfluorene) and is represented by pF. The composition ratio of oligothiophene units (x%) was controlled by changing the molar fractions of 2,7-dibromo-9,9'-di-n-octylfluorene and dibromo oligothiophene during synthesis. The elementary analysis indicates that the composition ratios were almost consistent with the thiophene fractions loaded in a reaction flask (Table 1).

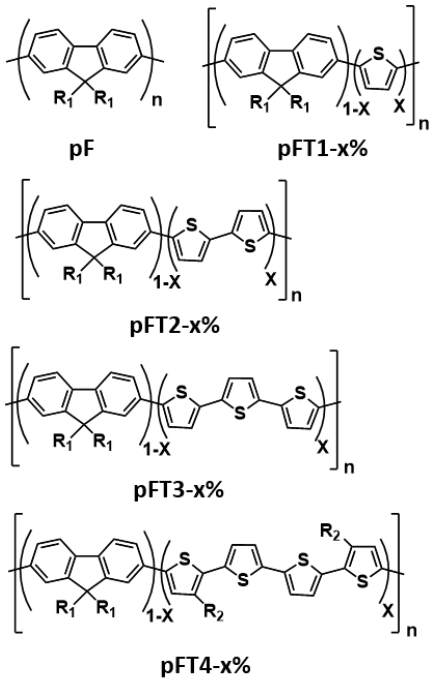

Figure 1. Structures of fluorene-thiophene copolymers: pFTn-x% (n = 0-4, x = 50, 25, 10, and 2%) synthesized by Suzuki-Miyaura coupling. R_1: n-octyl. R_2: n-hexyl.

Table 1. Polymeric properties of pFTn-x% copolymers.

synonym	M_w (10^4 g mol^{-1})	PDI	monomer unit
pF	5.7	2.4	146
pFT1-2%	4.1	2.1	107
pFT1-5%	6.6	2.0	182
pFT1-10%	3.6	1.8	116
pFT1-50%	0.5	1.2	21
pFT2-2%	4.0	2.2	104
pFT2-5%	5.3	2.2	144
pFT2-10%	4.5	2.1	133
pFT2-50%	4.2	2.1	153
pFT3-2%	4.4	2.1	113
pFT3-5%	7.6	2.3	202
pFT3-10%	6.5	2.7	184
pFT3-50%	0.7	1.6	22
pFT4-2%	4.3	2.2	111
pFT4-5%	4.8	1.9	120
pFT4-10%	7.2	2.2	172
pFT4-50%	6.6	2.1	148

1. 4. 2. Optical Properties of pFTn-x% Copolymer

Parts a-d of Figure 2 illustrate the steady-statephotoabsorption and fluorescence spectra of pFTn_x% (n = 0-4) in chloroform solutions having composition ratio, x = 2, 10, 25, and 50% respectively. The band gap energy of the copolymers was estimated from the band edge of the steady-state photoabsorption spectra and the fluorescence peak which are shown in parts e and f of Figure 2, respectively. As shown in Figure 2e, the band gaps of polymers gradually decreased from ca. 2.9 eV of pF to 2.3 eV of pFT4-50%. The fluorescence peaks of pFTn-2% (n = 1-4) shown in Figure 2f were almost identical to that of pF, although a small portion of fluorescence ascribed to the oligothiophene units could be observed at the longer wavelength region. By increasing the ratio of oligothiophene units (>10%) on the polymer backbone, the fluorescence peaks exhibited a distinct red shift with the number of oligothiophene (n). These results imply that excitons can migrate along the polyfluorene over 10 repeating units within their lifetimes, which is in good agreement with the efficient exciton migration along the chain reported in literature.[5]

1. 4. 3. Intramolecular Charge Carrier Mobility of pFTn-x% Copolymer by FP-TRMC Measurement

The transient photoconductivity of the copolymer films was measured by FP-TRMC using a 355 nm nanosecond laser as the excitation source. Figure 3a shows $\phi\Sigma\mu$ transients of pF and pFTn-50% (n = 1-4) films, where ϕ and $\Sigma\mu$ are the quantum efficiency of charge carrier generation and the sum of charge carrier mobilities ($\Sigma\mu = \mu_+ + \mu_-$), respectively. The primary charged species is presumed to be holes ($\Sigma\mu \approx \mu_+ \gg \mu_-$), since the field-effect transistor (FET) or time-of-flight (TOF) studies of pF and pFT2-50% (F8T2) exhibited p-type characteristics[4, 6, 12, 13] and $\phi\Sigma\mu$ transients were not influenced by air, argon, and

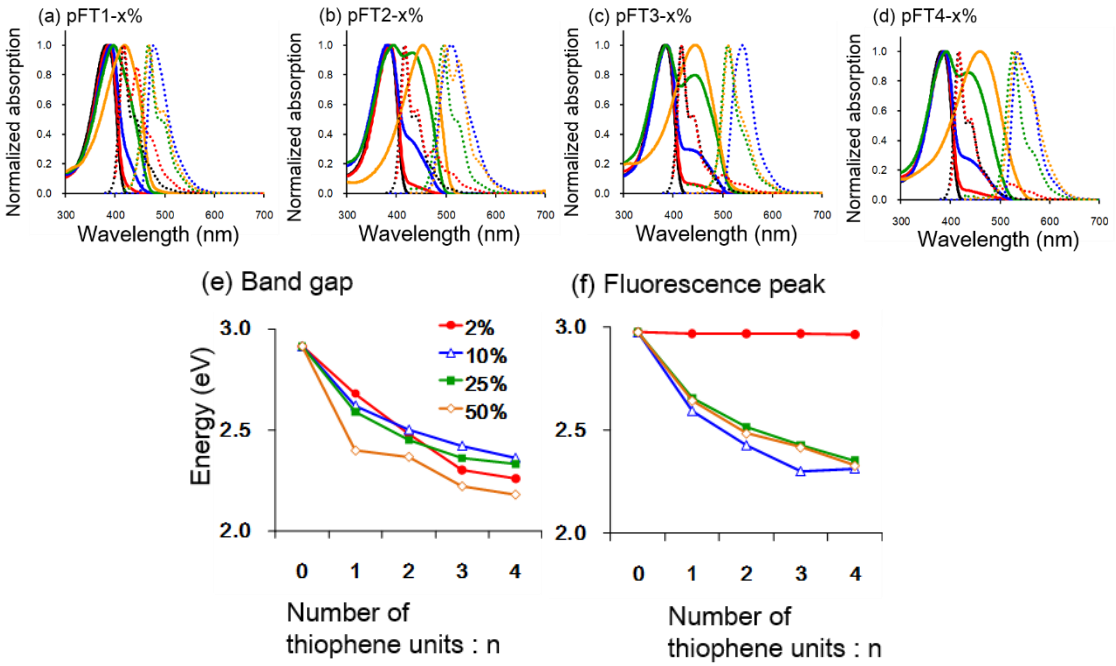

Figure 2. Steady-state photoabsorption (solid line) and fluorescence (dotted line) spectra (l_{ex} = 350 nm) of (a) pFT1-x%, (b) pFT2-x%, (c) pFT3-x%, and (d) pFT4-x% in chloroform having composition ratio, x = 0% (black), x = 2% (red), x = 10% (blue), x = 25% (green), and x = 50% (orange). The band gap energy of the copolymers estimated from (e) the band edge of the steady-state photoabsorption spectra and (f) the fluorescence peak.

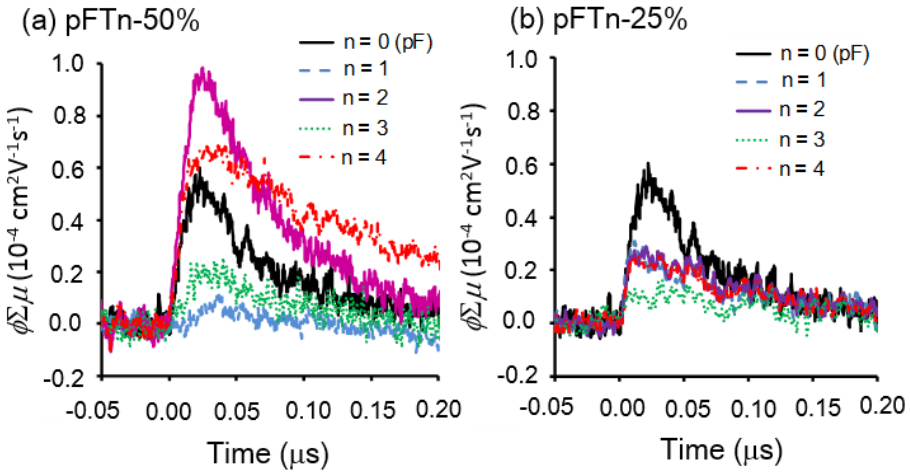

Figure 3. Photoconductivity transients of (a) pFTn-50% and (b) pFTn-25% films measured by FP-TRMC using 355 nm excitation(photon density = 9.1 × 10^{15} cm^{-2} $pulse^{-1}$). The solid black, bluedashed, purple solid, green dotted, and red dashed lines are n = 0-4, respectively.

SF6 gases. Except for pFT4-50%, all of the transients exponentially decayed after the end of pulse with a lifetime of ca. 60 ns. This exponential decay was also observed in pFTn-25% (Figure 3b) and other copolymers. Only pFT4-50% exhibited a slow decay which is fitted by second order dynamics rather than first order. Nevertheless, the decay rates of these kinetics were not accelerated by the increase of laser excitation power, as is the case of organic single crystals where the charge carriers decay through bimolecular recombination under their diffusive motions.[16] This result indicated that photogenerated charge carriers in fluorene-thiophene copolymers undergoes quick deactivation by trapping sites such as kinks and intermolecular/intersegment energy barriers.

The highest values of $\phi\Sigma\mu$ (i.e., $\phi\Sigma\mu_{max}$) in Figure 3 are therefore considered to reflect the intrinsic charge carrier mobility in the polymers with minimum trapping effects. Polyfluorene has been reported to exhibit a 1-dimensional intramolecular mobility as high as 0.7 $cm^2\ V^{-1}\ s^{-1}$ by pulse radiolysis-TRMC in an insulated and isolated matrix of benzene solution.[15] In contrast, the long-range mobilities are of in the order of 10^{-3}~10^{-4} $cm^2\ V^{-1}\ s^{-1}$ as estimated by TOF, [4] FET, [6] and transient photoabsorption spectroscopy.[8] One plausible explanation is that although the stiff backbones of polyfluorenes has a high intramolecular charge mobility on the planner π-orbitals along a relatively long Kuhn segments (segment length = 17.1 nm),[3] on a long-range the charge carriers immediately encounter barriers at the breaking point of π-conjugation and/or at the intermolecular hopping barriers. This can be also corroborated by considering the steric effect of alkyl chains at the 9-position of fluorene, which is perpendicular to the π-plane disturbs the close intermolecular packing. Besides, the neighboring fluorene units are rotated with a torsional angle of 41.6° as calculated by density functional theory (DFT).[7] Nevertheless, the high potential of 1-dimensional intramolecular mobility of polyfluorene motivated to

investigate the effect of incorporated thiophene units on the intramolecular charge transport properties of polyfluorene.

To determine $\Sigma\mu$ of each copolymer, a directcurrent (DC) method in which an interdigitated comb-type gold electrode with 5 μm gaps were used to measure directly the photocurrent generated by 355 nm excitation in spun-cast films under an applied bias of 2×10^4 V cm^{-1} was utilized.[18] ϕ of pF was calculated on the basis of known 1-dimensional mobility ($\Sigma\mu_{1D}$)[15] as assessed by TRMC in a benzene solution. The ϕ of other copolymers were calibrated by the obtained ϕ of pF (2.3×10^{-4}, Table 1).

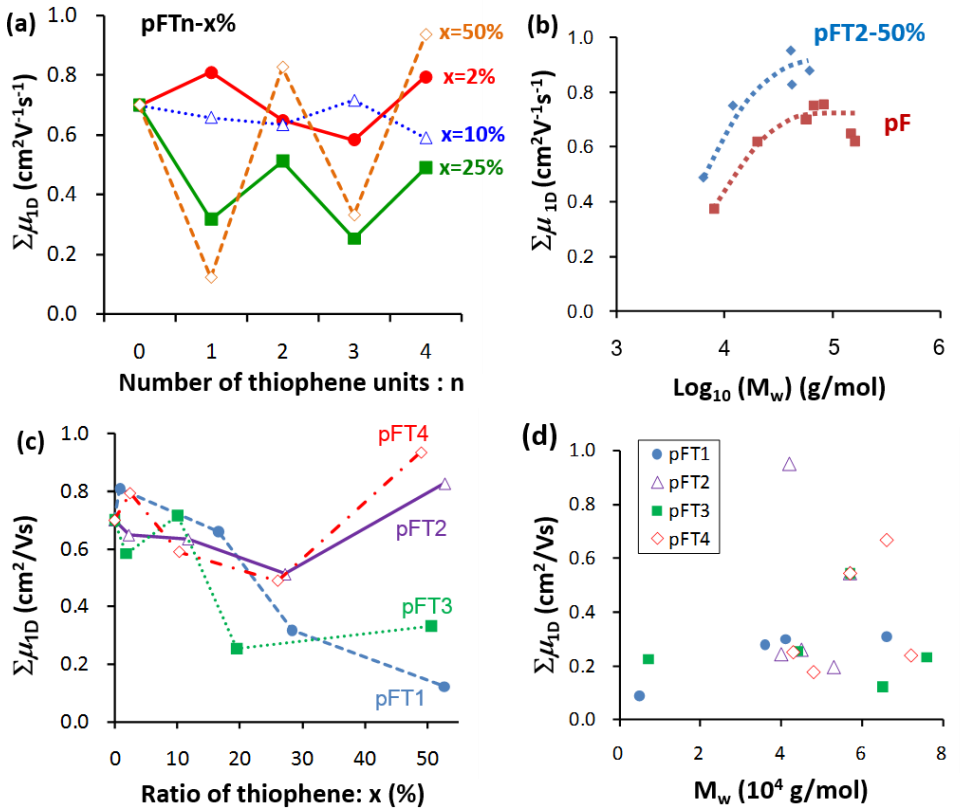

Figure 4. 1-dimensional charge carrier mobility ($\phi\Sigma_{1D}$) of pFTn-x% films estimated from the combination of FP-TRMC and DC techniques. (a) $\phi\Sigma_{1D}$ vs the number of thiophene unit. (b) $\phi\Sigma_{1D}$ vs logarithmic plot of weight-averaged molecular weight (M_w). (c) $\phi\Sigma_{1D}$ are plotted as a function of the composition ratio of thiophene (x%). The values obtained by elementary analysis were used as x%. (d) $\phi\Sigma_{1D}$ are plotted vs M_w without distinguishing the values of x%.

Figure 4a shows $\Sigma\mu_{1D}$ of copolymers plotted against the number of thiophene units. The value of $\phi\Sigma\mu_{max}$ and ϕ_{max} used to calculate $\Sigma\mu_{1D}$ are presented in Table 1. The plot of pFTn-50% indicates an "odd-even effect" in which $\Sigma\mu_{1D}$ of the polymers containing odd-numbers thiophene unit (n = 1 and 3) were significantly smaller than the polymers with even numbers of thiophene (n = 0, 2, and 4); however, it should be noted that the effect of the small molecular weight might be convoluted in this result, since the weight-averaged molecular weights (M_w) of pFT1-50% and pFT3-50% are nearly 1 order smaller than the others. These copolymers with high M_w were not successfully synthesized, presumably due to the low reactivity of dibromo thiophene, low solubility of terthiophene, and as well as the conformational disadvantage of the odd-number oligothiophene units (vide infra). We examined the impact of M_w on $\Sigma\mu_{1D}$ by preparing pF and pFT2-50% with low and high molecular weights. The increased with M_w mainly due to the increase of ϕ_{max}. The obtained $\Sigma\mu_{1D}$ of both pF and pFT2-50% clearly exhibits an increase followed by a saturation at high M_w (Figure 4b). $\Sigma\mu_{1D}$ values of these polymers were roughly half of each saturated values at M_w = ca. 5×10^3 g mol^{-1} which is close to those of pFT1-50% and pFT3-50%. Therefore, the mobilities of the even-numbered copolymer were still higher than odd numbers, when one compares $\Sigma\mu_{1D}$ at a low M_w.

In order to further confirm the odd-even effect, $\Sigma\mu_{1D}$ of polymers with lower composition ratio of oligothiophene were measured in the same manner. $\Sigma\mu_{1D}$ of pFTn-25% (n = 0-4) was also found to be affected by the odd-even numbers of thiophene units. On the other hand, this effect was almost disappeared for pFTn-10% and pFTn-2%, where their $\Sigma\mu_{1D}$ resembled the values of pF. From the plot of $\Sigma\mu_{1D}$ as a function of the composition ratio, it is clear that the odd-even effect becomes predominant for x > ca. 20% (Figure 4c). The $\Sigma\mu_{1D}$ plot of all copolymers plotted against their M_w is a quite

intuitive representation, wherein $\Sigma\mu_{1D}$ increased roughly with M_w, but they are scattered. (Figure 4d).

1. 4. 4. FP-TRMC and TAS Measurement of pFTn-x% in PS Matrix

As described above, $\Sigma\mu_{1D}$ values were estimated from FP-TRMC and DC measurements

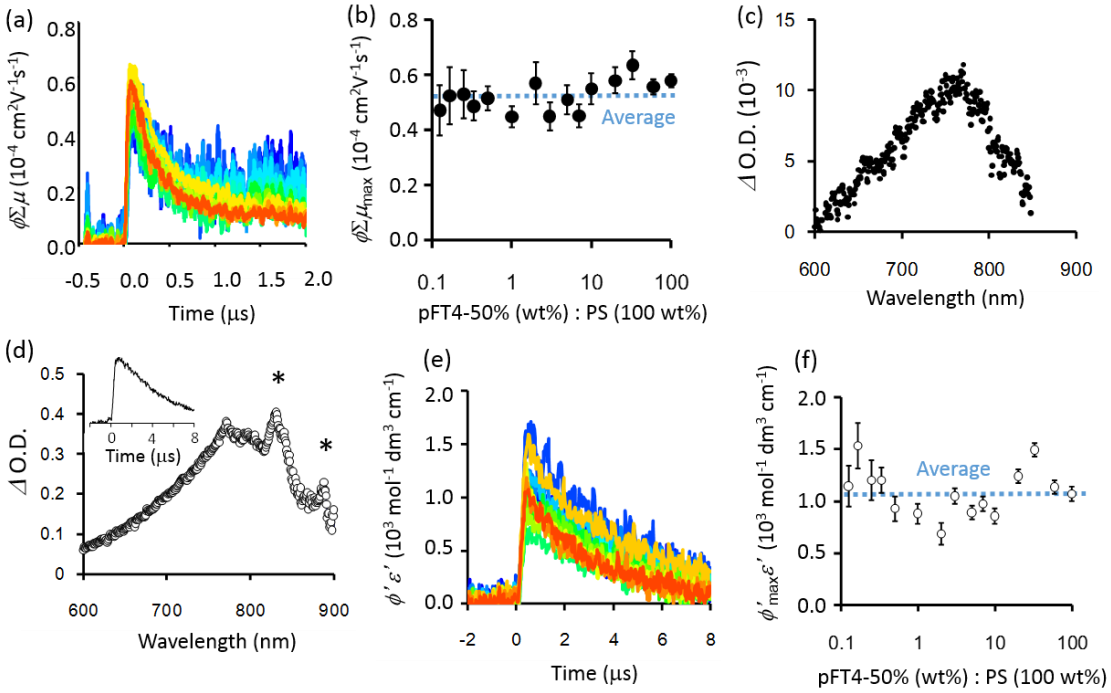

Figure 5. FP-TRMC and TAS studies of the blend films of pFT4-50% and polystyrene (PS) under the excitation at 355 nm. (a) FP-TRMC transients of the blend films (pFT4-50% : PS = 0.013 (blue), 100 (red) : 100 w/w). The difference in the absorbance of each film was compensated according to the reported procedure.[19] (b) Peak of FP-TRMC transients ($\phi\Sigma\mu_{max}$) vs pFT4-50% concentration. The dotted line represents the averaged $\phi\Sigma\mu_{max}$. (c) Transient absorption spectrum (optical density : O.D.) of pFT4-50% : PS = 100:100 film. No significant changes were observed in other blend films. (d) Transient absorption spectrum observed in N_2-bubbled toluene solution of pFT4-50% (1.5 mg mL^{-1}). The peaks labeled by asterisk were artificial, arisen from the characteristic bright line of a Xe lamp. The inset shows the kinetic profile at 760 nm. (e) TAS kinetics of the blend films (pFT4-50% : PS = 0.013 (blue), 100 (red) : 100 w/w) monitored at 750 nm. See text for the explanation on ϕ' and ε'. (f) Plot of (ϕ'_{max} ε') vs pFT4-50% concentration. The dotted line represents the averaged ϕ'_{max} ε'.

of pristine films on the basis of the reported $\Sigma\mu_{1D}$ of pF in benzene solution. However, one might cast doubt on the validity of this method by assuming some contribution from intermolecular charge carrier mobility along with the intramolecular process. Hence to rule out this possibility, pFT4-50% and polystyrene (PS) mixed films were prepared by changing the blend ratio from 0.013 to 100 wt % of pFT4-50% relative to 100 wt % PS. We have confirmed that the PS was unable to give a distinct FP-TRMC and transient absorption spectroscopy (TAS) signals on the excitation at 355 nm and also possess a good compatibility with conjugated polymers. Figure 5a shows $\phi\Sigma\mu$ decays observed in the blend films. The difference in the absorbance of each film was compensated according to the reported procedure.[19] Increase of pFT4-50% concentration in PS matrix led to the slight acceleration of the decay rate, probably due to the increase in the density of charge trapping sites. It is of importance that an almost constant $\phi\Sigma\mu_{max}$ werer observed over the wide range of blend ratio as shown in Figure 5b. The averaged $\phi\Sigma\mu_{max}$ was ca. 0.52×10^{-4} cm^2 V^{-1} s^{-1},which was close to the value obtained for the pristine pFT4-50% film (0.67×10^{-4} cm^2 V^{-1} s^{-1}). This proves that FP-TRMC mainly probes the intramolecular charge carrier mobility even in the pristine films.

PS acts an insulating matrix, which cannot be used for DC measurements to estimate the charge carrier generation efficiency of the blend films. Therefore, TAS analysis on the blend film on excitation at 355 nm was performed and a clear transient absorption spectrum centered at ca. 750 nm was found as shown in Figure 5c. The spectrum shape was not varied by the blend ratio. Figure 5d displays a transient absorption spectrum observed in N_2-saturated toluene solution of pFT4-50%. The absorption maximum is located at ca. 760 nm and the decay follows a first order kinetics with a lifetime of 4.6 μs. The absorption was quenched by O_2-bubbling, confirming that the transient was due to a

triplet excited state. The decay profiles observed at 750 nm in the pFT4-50% : PS blend films are shown in Figure 5e, where the vertical axis represents the product of quantum yield (ϕ') and extinction coefficient (ε') of an *intermediate species*, derived from the observed transient photoabsorption, film thickness, steady state photoabsorption at the excitation wavelength, and TAS geometry, according to the reported procedure.[19] All of the profiles were fitted by a first order decay, giving lifetime values in the range of 2.8 - 4.4 μs (the average was 3.8 μs) which is much longer than the decay of FP-TRMC transients (Figure 5a). Although both radical cation and anion have the absorption maxima at ca. 790 nm, the absorption found in the pFT4-50%:PS blend films was ascribable mainly to the triplet state by considering the lifetime and the spectrum peak. The maximum $\phi'\varepsilon'$ (= $\phi'_{max}\varepsilon'$) was extracted and plotted as a function of pFT4-50% concentration in Figure 5f. No distinct trend could be observed, indicating that the triplet quantum yield is not changed significantly by the blend ratio, suggesting that the charge carrier generation efficiency ϕ does not vary considerably with the latter.

1. 4. 5. Study of Odd-Even Effect of pFTn-x%

Since the thiophene ring has a bended bond direction at its 2 and 5 positions, its incorporation in odd and even numbers in a polymer backbone could lead to different molecular packing in crystalline phase. There are several reports based on the dependence of odd-even effects on thermal, optical, and electrical properties of conjugated materials. For example, it has been reported that the crystal densities of the even-numbered oligothiophenes are slightly higher than those of odd-number.[20] The systematic investigation on the effect of odd-even numbers of thiophene units on the bulk crystalline properties were reported by Clot et al. in oligothiophenes (n = 1-6) capped with two

dibutylaminostyryl moieties, where they observed an increase in the melting points of even-numbered oligomers (about 50 ^{o}C) when compared to that of odd-numbered ones. [21] Regarding the electronic properties, Nagamatsu et al.[22] have performed FET studies on unsubstituted oligothiophenes (n = 5-7), showing that the FET mobilities of even-numbered oligothiophenes were improved, due to the proper structural ordered arrangement. Bao's group[23] has demonstrated better FET mobilities of the even-numbered 5,5'-bis(7-hexyl-9*H*-fluoren-2-yl)-2,2'-oligothiophenes (n = 1-4). He et al.[24] have synthesized the fused thiophene (n = 3-5) and bithiophene copolymers and showed that the FET mobilities of even-numbered derivatives were superior to those of odd-numbered derivatives. All of these reports dealt with the advantage of even-numbered thiophenes in the intermolecular charge transport, which arises due to the favorable packing of their crystalline structures. In contrast, the intramolecular charge mobility would be affected mainly by the feature of a single polymer chain rather than its packing structure.

The chain conformations of F-T copolymers were established with density functional theory (DFT) using B3LYP/6-31G(d, p) level. The torsional potential energy profiles of neutral states of fluorene-thiophene-fluorene trimers were calculated. One of the fluorene units was rotated after the geometry optimization (Figure 6a). As shown in Figure 6b, the neutral pF trimer has a minimum energy at the torsion angle (θ) of 37^{o} due to the repulsive force of protons of neighboring aromatic rings, while the other trimers take more planar structures with the minimum θ of 24^{o}-30^{o}. This planarity of pFTn (n = 1-4) trimers is more pronounced for their cationic states. These results rationalize the slightly higher $\Sigma\mu_{1D}$ of pFT2-50% and pFT4-50% than that of pF (Figure 4a). The $\Sigma\mu_{1D}$ decreased by increasing the composition ratio of fluorene units which insert a twisted site into the

copolymer backbone. The DFT calculations of the neutral states were, however, not indicative of the odd-even effect in the minimum θ, the relative energies at θ = 0 and 180° (Figure 5c), and the potential barriers of the rotation at θ = 90° (3-4 kcal mol^{-1}).

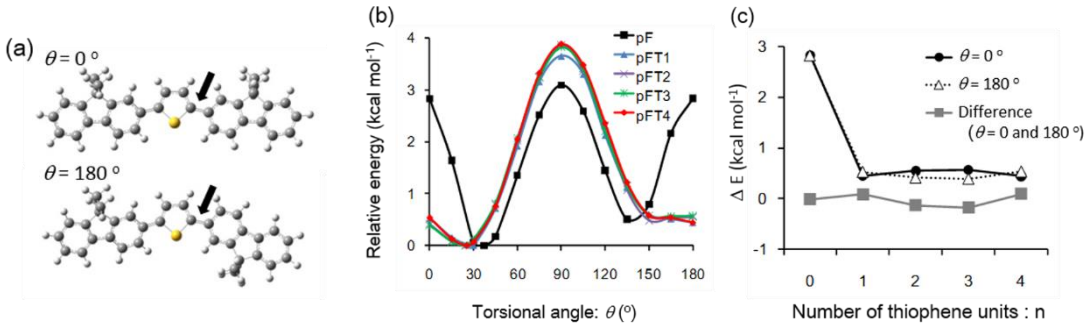

Figure 6. (a) Snapshots of pFT1 trimer with torsional angle q of 0 and 180°. The molecular geometry was optimized by DFT using B3LYP/6-31G(d, p) level. The fluorene unit was rotated along the arrowed bond. (b) Torsional potential energy profiles of neutral states of pFTn trimmers (n = 0-4). The alkyl chains were replaced by methyl substituent for simplicity. (c) The relative energy (ΔE) at q = 0° (black filled circle and black solid line) and 180° (open triangle and black dotted line). The gray square and line indicate the energy difference between q = 0 and 180°.

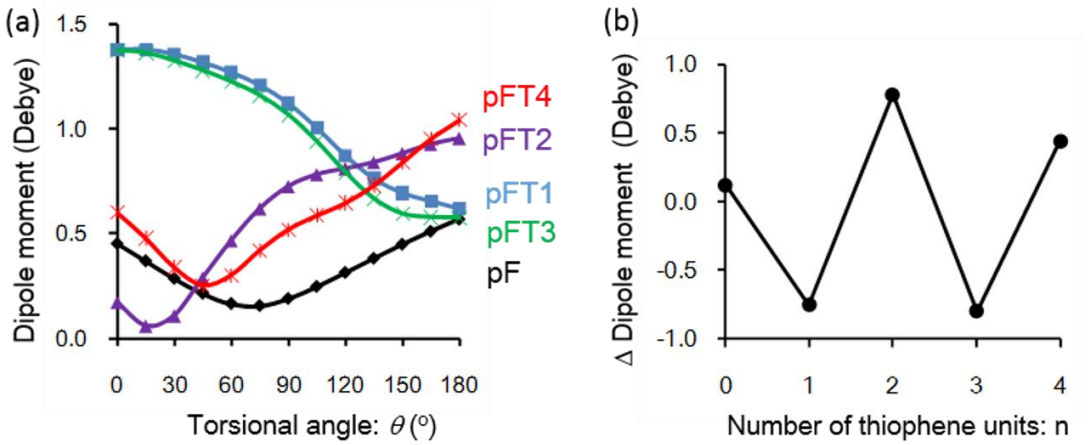

Figure 7. (a) Dipole moments of neutral states of pFTn trimmers (n = 0-4) vs torsional angle calculated with DFT using B3LYP/6-31G(d,p) level. (b) Difference of dipole moments between 0 and180°.

Since both thiophene and fluorene units have a tilted angle of bond direction, the direction

of dialkyl chains at the fluorene unit might be affected by the number of oligothiophene units. As shown in Figure 6a, the alkyl chains were placed at one side for the odd-numbered copolymers (e.g., pFT1), while they occupy at opposite sides in the even-numbered copolymers (e.g., pFT2) when the conjugated units were aligned in a straight manner ($\theta = 0^{o}$). The energy difference between $\theta = 0$ and 180^{o} was estimated as small as ca. 0.4 kcal mol^{-1} by the DFT, suggesting that both conformations are stable. However, the linearity of polymer backbone is largely affected by the parity of oligothiophene units. This is visualized by the relative change of dipole moments of trimers, whereas the odd-numbered trimers showed a decrease of dipole by the rotation from $\theta = 0$ to 180^{o} in contrast to an increase for the even-numbered trimers (Figure 7). The alkyl side chains of conjugated polymers have been known for not only to improve their solubility but also to change the backbone conformations, leading to solvatochromism, thermochromism, etc.[25] The rotation of the fluorene units in a an odd-numbered pFTn to make the alkyl chains in opposite directions to maximize the interaction with solvents distorts the polymer backbone as shown in the lower part of Figure 6a and hence reduces the charge carrier motion parallel to the direction of electric field of probing microwave. The drawback of shrunk conformation of main chain was also confirmed from the FP-TRMC experiment, in which photoconductivity of pFT2-50% powder precipitated in methanol was decreased to ca. 30% of the film (Figure 8).

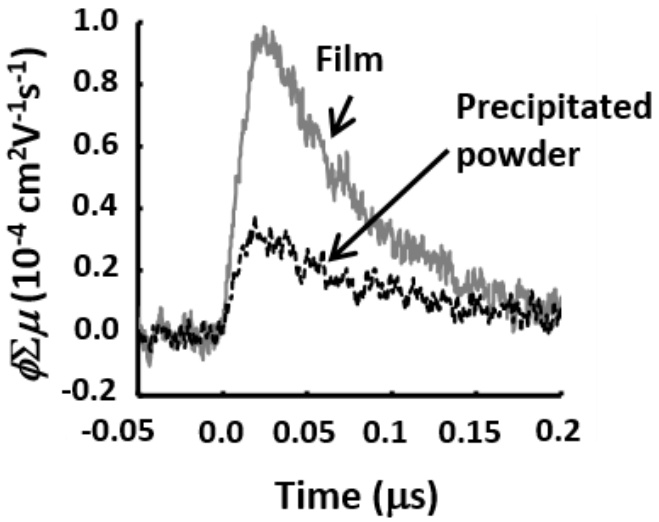

Figure 8. Photoconductivity transients of pFT2-50% films and pFT2-50% powder precipitated in methanol by FP-TRMC.

1. 5. Conclusion

The intramolecular mobilities of charge carrier in fluorene-thiophene copolymer films were investigated by FP-TRMC technique. The important observation was that the charge carrier mobilities of copolymers with the even-numbered oligothiophene units with composition ratios of 50 and 25% are higher than those of the odd-number polymers. This is correlated with the tilted bond direction of thiophene and fluorene rings and the resultant alternating symmetry of the alkyl chains at the fluorene unit. Interestingly, this odd-even effect disappeared and the mobility converged to ca. 0.7 cm^2 V^{-1} s^{-1} once the oligothiophene composition ratio was decreased to less than 10%. It should be emphasized that the mobility decreases in the polymers with M_w less than 10^4 g mol^{-1}. We do hope these findings are extremely important from the point of view of designing copolymers for various applications like OPV and OLED.

1. 6. References and notes

[1] (a) Coropceanu, V.; Cornil, J.; da Silva Filho, D. A.; Olivier, Y.; Silbey, R.; Brédas, J.-L. *Chem. Rev.* **2007**, *107*, 926. (b) Argun, A. A.; Aubert, P.-H.; Thompson, B. C.; Schwendeman, I.; Gaupp, C. L.; Hwang, J.; Pinto, N. J.; Tanner, D. B.; MacDiarmid, A. G.; Reynolds, J. R. *Chem. Mater.* **2004**, *16*, 4401. (c) Wheeler, S. E.; McNeil, A. J.; Műller, P.; Swager, T. M.; Houk, K. N. *J. Am. Chem. Soc.* 2010, 132, 3304. (d) Tulek, A.; Polson, R. C.; Vardeny, Z. V. *Nature Phys.* 2010, 6, 303.

[2] (a) Kim, J. Y.; Lee, K.; Coates, N. E.; Moses, D.; Nguyen, T.-Q.; Dante, M.; Heeger, A. J. *Science* **2007**, *317*, 222. (b) Inganäs, O.; Zhang, F.; Andersson, M. R. *Acc. Chem. Res.* **2009**, *42*, 1731. (c) Dennler, G.; Scharber, M. C.; Brabec, C. *J. Adv. Mater.* **2009**, *21*, 1323. (d) Bijleveld, J. C.; Zoombelt, A. P.; Mathijssen, S. G. J.; Wienk, M. M.; Turbiez, M.; de Leeuw, D. M.; Janssen, R. A. J. *J. Am. Chem. Soc.* **2009**, *131*, 16617. (e) Chen, H. -Y.; Hou, J.; Zhang, S.; Liang, Y.; Yang, G.; Yang, Y.; Yu, L.; Wu, Y.; Li, G. *Nature Photon.* **2009**, *3*, 649. (f) Piliego, C.; Holcombe, T. W.; Douglas, J. D.; Woo, C. H.; Beaujuge, P. M.; Fréchet, J. M. J. *J. Am. Chem. Soc.* **2010**, *132*, 7595. (g) Jiang, Y.; Okamoto, T.; Becerril, H. A.; Hong, S.; Tang, M. L.; Mayer, A. C.; Parmer, J. E.; McGehee, M. D.; Bao, Z. *Macromolecules* **2010**, *43*, 6361.

[3] Grell, M.; Bradley, D. D. C.; Long, X.; Chamberlain, T.; Inbasekaran, M.; Woo, E. P.; Soliman, M. *Acta Polym.* **1998**, *49*, 439.

[4] Redecker, M.; Bradley, D. D. C.; Inbasekaran, M.; Woo, E. P. *Appl. Phys. Lett.* **1999**, *74*, 1400.

[5] (a) Lyons, B. P.; Monkman, A. P. *Phys. Rev. B* **2005**, *71*, 235201. (b) Shibano, Y.; Imahori, H.; Sreearunothai, P.; Cook, A. R.; Miller, J. R. J. *Phys. Chem. Lett.* **2010**, *1*, 1492.

[6] Yasuda, T.; Fujita, K.; Tsutsui, T.; Geng, Y.; Culligan, S. W.; Chen, S. H. *Chem. Mater.* **2005**, *17*, 264.

[7] Fratiloiu, S.; Grozema, F. C.; Koizumi, Y.; Seki, S.; Saeki, A.; Tagawa, S.; Dudek, S. P.; Siebbeles, L. D. A. J. *Phys .Chem. B* **2006**, *110*, 5984.

[8] Asaoka, S.; Takeda, N.; Iyoda, T.; Cook, A. R.; Miller, J. R. *J. Am. Chem. Soc.* **2008**, *130*, 11912.

[9] (a) Moynihan, S.; Lovera, P.;O'Carroll, D.; Iacopino, D.; Redmond, G. *Adv. Mater.* **2008**, *20*, 2497. (b) Scherf, U.; Gutacker, A.; Koenen, N. *Acc. Chem. Res.* **2008**, *41*, 1086. (c) Simon, S. C.; Schmaltz, B.; Rouhanipour, A.; Räder, H. J.; Müllen, K. *Adv. Mater.* **2009**, *21*, 83. (d) Tachibana, Y.; Makuta, S.; Otsuka, Y.; Terao, J.; Tsuda, S.; Kambe, N.; Seki, S.; Kuwabata, S. *Chem. Commun.* **2009**, *29*, 4360. (e) Zhou, E.; Cong, J.; Yamakawa, S.; Wei, Q.; Nakamura, M.; Tajima, K.; Yang, C.; Hashimoto, K. *Macromolecules* **2010**, *43*, 2873.

[10] Tu, G.; Li, H.; Forster, M.; Heiderhoff, R.; Balk, L. J.; Sigel, R.; Scherf, U. *Small* **2007**, *3*, 1001.

[11] (a) Yao, K.; Chen, Y.; Chen, L.; Zha, D.; Li, F.; Pei, J.; Liu, Z.; Tian, W. *J. Phys. Chem. C* **2010**, *114*, 18001. (b) Bu, L.; Guo, X.; Yu, B.; Qu, Y.; Xie, Z.; Yan, D.; Geng, Y.; Wang, F. *J. Am. Chem. Soc.* **2009**, *131*, 13242. (c) Shi, C.; Yao, Y.; Yang, Y.; Pei, W. *J. Am. Chem. Soc.* **2006**, *128*, 8980.

[12] Sirringhaus, H.; Wilson, R. J.; Friend, R. H.; Inbasekaran, M.; Wu, W.; Woo, E. P.; Grell, M.; Bradley, D. D. C. *Appl. Phys. Lett.* **2000**, *77*, 406.

[13] Morana, M.; Bret, G.; Brabec, C. *Appl. Phys. Lett.* **2005**, *87*, 153511.

[14] (a) Lu, G.; Usta, H.; Risko, C.; Wang, L.; Facchetti, A.; Ratner, M. A.; Marks, T. J. *J. Am. Chem. Soc.* **2008**, *130*, 7670. (b) Werzer, O.; Matoy, K.; Smilgies, D.-M.;

Rothmann, M. M.; Strohriegl, P.; Resel, R. *J. Appl. Polym. Sci*. **2008**, *107*, 1817.

[15] (a) Grozema, F. C.; Siebbeles, L. D. A.; Warman, J. M.; Seki, S.; Tagawa, S.; Scherf, U. *Adv. Mater.* **2002**, *14*, 228. (b) Grozema, F. C.; Warman, J. M. Radiat. *Phys. Chem.* **2005**, *74*, 234.

[16] Saeki, A.; Seki, S.; Takenobu, T.; Iwasa, Y.; Tagawa, S. *Adv. Mater.* **2008**, *20*, 920.

[17] (a) Yamamoto, Y.; Zhang, G.; Jin, W.; Fukushima, T.; Ishii, N.; Saeki, A.; Seki, S.; Tagawa, S.; Minari, T.; Tsukagoshi, K.; Aida, T. *Proc. Natl. Acad. Sci.* **2009**, *106*, 21051. (b) Kocherzhenko, A. A.; Patwardhan, S.; Grozema, F. C.; Anderson, H. L.; Siebbeles, L. D. A. *J. Am. Chem. Soc.* **2009**, *131*, 5522. (c) Pingel, P.; Zen, A.; Abellón, R. D.; Grozema, F. C.; Siebbeles, L. D. A.; Neher, D. *Adv. Funct. Mater.* **2010**, *20*, 2286. (d) Saeki, A.; Seki, S.; Shimizu, Y.; Yamao, T.; Hotta, S. *J. Chem. Phys.* **2010**, *132*, 134509.

[18] (a) Ie, Y.; Nitani, M.; Uemura, T.; Tominari, Y.; Takeya, J.; Honsho, Y.; Saeki, A.; Seki, S.; Aso, Y. *J. Phys. Chem. C* **2009**, *113*, 17189. (b) Zhang, W.; Ochi, K.; Fujiki, M.; Naito, M.; Ishikawa, M.; Kaneto, K..; Takashima, W.; Saeki, A.; Seki, S. *Adv. Funct. Mater.* **2010**, *20*, 3941. (c) Terao, J.; Tanaka, Y.; Tsuda, S.; Kambe, N.; Taniguchi, M.; Kawai, T.; Saeki, A.; Seki, S. *J. Am. Chem. Soc.* **2009**, *131*, 18046.

[19] (a) Saeki, A.; Seki, S.; Koizumi, Y.; Tagawa, S. *J. Photochem. Photobiol. A* **2007**, *186*, 158. (b) Saeki, A.; Seki, S.; Sunagawa, T.; Ushida, K.; Tagawa, S. *Phil. Mag.* **2006**, *86*, 1261.

[20] (a) Barbarellu, G.; Casarini, D.; Zambianchi, M.; Favaretto, L.; Rossini, S. *Adv. Mater.* **1996**, *8*, 69. (b) Azumi, R.; Goto, M.; Honda, K.; Matsumoto, M. *Bull. Chem. Soc. Jpn.* **2003**, *76*, 1561. (c) Melucci, M.; Gazzano, M.; Barbarella, G.; Cavallini, M.; Biscarini, F.; Maccagnani, P.; Ostoja, P. *J. Am. Chem. Soc.* **2003**, *125*, 10266.

[21] Clot, O.; Selmarten, D.; McNevin, M. J. *J. Mater. Chem.* **2005**, 15, 4934.

[22] Nagamatsu, S.; Kaneto, K.; Azumi, R.; Matsumoto, M.; Yoshida, Y.; Yase, K. *J. Phys. Chem. B* **2005**, *109*, 9374.

[23] Meng, H.; Zheng, J.; Lovinger, A. J.; Wang, B. C.; Van Patten, P. G.; Bao, Z. *Chem. Mater.* **2003**, *15*, 1778.

[24] He, M.; Li, J.; Sorensen, M. L.; Zhang, F.; Hancock, R. R.; Fong, H. H.; Pozdin, V. A.; Smilgies, D.-M.; Malliaras, G. G. *J. Am. Chem. Soc.* **2009**, *131*, 11930.

(25) (a) Leclerc, M.; Faid, K. *Adv. Mater.* **1997**, *9*, 1087. (b) Bolognesi, A.; Giacometti Schieroni, A.; Botta, C.; Marinelli, M.; Mendichi, R.; Rolandi, R.; Relini, A.; Inganäs, O.; Theandher, M. *Synth. Met.* **2003**, *139*, 303.

Chapter 2

Charge Carrier Mobilities in Amorphous Triphenylamine–Fluorene Copolymers: Role of Triphenylamine Unit in Intra- and Intermolecular Charge Transport

2. 1. Abstract

The effect of the triphenylamine (TPA) content of TPA–fluorene copolymers on their charge carrier mobilities was investigated. Intramolecular mobilities were measured by flash-photolysis time-resolved microwave conductivity (FP-TRMC), while intermolecular hole mobilities were determined on the basis of space-charge limited current (SCLC) and field-effect transistor (FET). FP-TRMC and SCLC except for FET showed an analogous dependence on the TPA content. The results are discussed from the viewpoints of delocalization of singly-occupied molecular orbital of radical cation, conformation of polymer chain, and trap effect. This study highlights the importance of optimizing the TPA content in the polyfluorene backbone for electronic device application.

2. 2. Introduction

Pi (π) conjugated copolymers have shown excellent photophysical and electrical properties relevant to their use in organic light-emitting diodes (OLED), although the underlying fundamental sciences are still being investigated vigorously. A stable and efficient electroluminescence (EL) in the primary colors, that is, red, green, and blue, must be guaranteed in the practical use. Among the large class of semiconducting organic conjugated polymers, triphenylamine (TPA) and fluorene (FL)-based copolymers occupy a unique place in OLED[1-4] and organic photovoltaic cells (OPV),[5, 6] because the TPA is an efficient hole transporting unit (i.e., it acts as a donor). Thanks to this, analogous molecules, for instance, N,N'-diphenyl-N,N'-bis(3-methylphenyl)-(1,1'-biphenyl)-4,4'-diamine (TPD),[6-8] N,N'-bis(1-naphthyl)-N,N'-diphenylbenzidine (α-NPD),[9, 10] and TPA dendrimers[11, 12] have been utilized as a hole transport layer in OLED. In this work, intra- and intermolecular charge carrier mobilities of TPA–FL copolymers was investigated, where the TPA content was changed discretely from 0 to 100%. These mobility measurements are implemented using flash-photolysis time-resolved microwave conductivity (FP-TRMC),[13, 14] space-charge limited current (SCLC),[15-17] and field-effect transistor (FET), allowing the examination of the role of TPA in the charge carrier transport.

2. 3. Result and Discussion

2. 3. 1. Synthesis and Polymeric properties of TPA-FL Copolymers

The TPA–FL copolymers shown in Figure 1 were synthesized via Suzuki coupling similarly to that described in a previous report.[13] The TPA content in the copolymers was controlled by changing the molecular fractions of reactant monomers. The resultant copolymers were FL_{100} [i.e., poly(9,9'-dioctylfluorene)], $TPA_{10}FL_{90}$, $TPA_{30}FL_{70}$, $TPA_{50}FL_{50}$, $TPA_{70}FL_{30}$, and TPA_{100}. As listed in Table I, theweight-averaged molecular weights (M_w) exceed 1.5×10^4 g/mol for all copolymers, which is large enough to neglect the M_w effect on the charge carrieir mobilities of FP-TRMC[13] and FET.[2] The polymers were dissolved in chlorobenzene at 1wt% concentration and drop-cast on quartz plates, which were used for the electrode-less photoconductivity measurement by FP-TRMC.

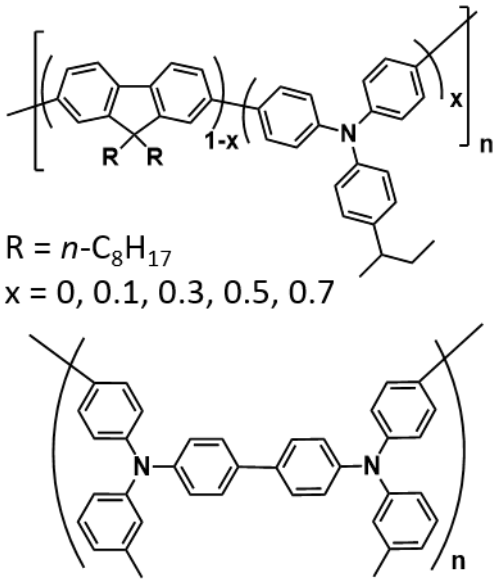

Figure 1. Chemical structures of TPA–FL copolymers. Upper: FL_{100} (x = 0), $TPA_{10}FL_{90}$ (x = 0.1), $TPA_{30}FL_{70}$ (x = 0.3), $TPA_{50}FL_{50}$ (x = 0.5), and $TPA_{70}FL_{30}$ (x = 0.7). Lower: TPA_{100}.

2. 3. 2. Intramolecular Charge Carrier Mobility of TPA-FL Copolymers

Figure 2a shows the FP-TRMC transient photoconductivity of the copolymers induced upon exposure to a 355 nm nanosecond laser. The $\phi\Sigma\mu$ represents the product of the charge carrier generation efficiency (ϕ) and the sum of hole and electron mobilities ($\Sigma\mu = \mu_h + \mu_e$). Interestingly, all the kinetic traces showed a fast mono-exponential decay, suggesting a prompt charger carrier immobilization by traps. In contrast, the maximum $\phi\Sigma\mu$ value ($\phi\Sigma\mu_{max}$) decreased and then increased with the TPA content. For the determination of $\Sigma\mu$, a direct-current technique with an interdigitated comb-type gold electrode with 5 μm gaps was used to estimate ϕ_{max} directly from the transient

Table 1. Charge carrier mobility and polymeric property

TPA content (%)	M_w (kg/mol)	PDI	$\phi\Sigma\mu_{max}$ (10^{-4} $cm^2V^{-1}s^{-1}$)	$\Sigma\mu_{1D}$ ($cm^2V^{-1}s^{-1}$)	$\mu_{h,SCLC}$ ($cm^2V^{-1}s^{-1}$)	$\mu_{h,FET}$ ($cm^2V^{-1}s^{-1}$)
0	76	3.2	2.1	0.76	5.1×10^{-7}	5.2×10^{-6}
10	80	1.8	1.7	0.67	2.0×10^{-6}	9.8×10^{-7}
30	210	2.4	2.0	0.79	2.5×10^{-6}	1.7×10^{-6}
50	140	2.2	0.90	0.38	5.8×10^{-7}	4.5×10^{-5}
70	300	5.4	0.42	0.28	6.2×10^{-8}	5.2×10^{-6}
100	15	2.7	1.7	0.71	1.8×10^{-7}	1.5×10^{-6}

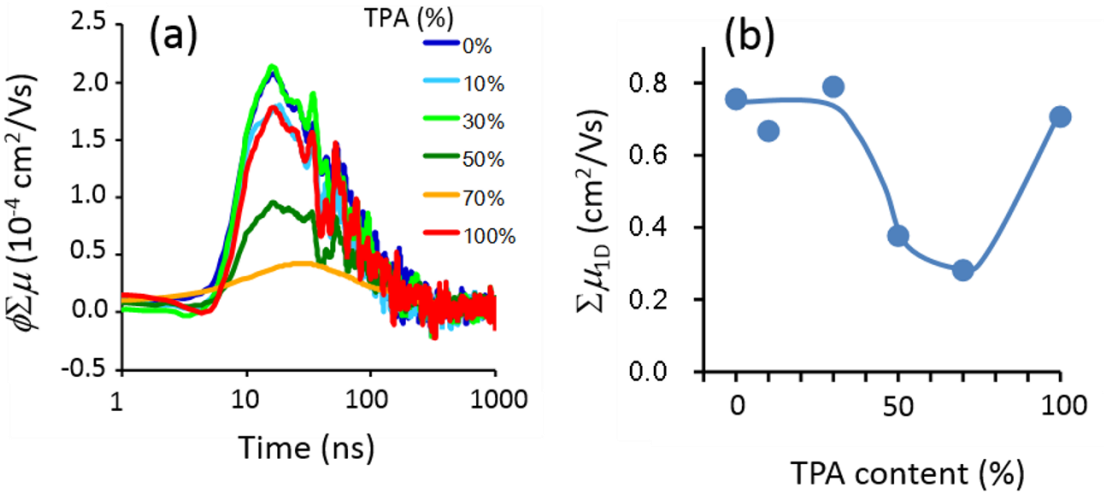

Figure 2. (a) FP-TRMC transients of TPA–FL copolymers induced by 355 nm laser excitation with incident photon density of 9.1×10^{15} photons cm^{-2}. (b) One-dimensional charge carrier mobility: $\Sigma\mu_{1D}$ vs TPA content.

photocurrent in spun-cast films under an applied bias of 2×10^4 Vcm^{-1}.[13] $\Sigma\mu$ was calculated by dividing $\phi\Sigma\mu_{max}$ by ϕ_{max}. Subsequently, one-dimensional charge carrier mobility along a polymer chain, $\Sigma\mu_{1D}$, was derived from $3 \times \Sigma\mu$. The measurement of intramolecular charge carrier mobility is possible because of the two reasons: (1) FP-TRMC can selectively probe the highest part of the charge carrier motion, i.e., along the main chain even in the bulk film, and (2) amorphous conjugated polymers show the same $\phi\Sigma\mu_{max}$, even though intermolecular interactions are removed by diluting the polymers in an insulating polystyrene matrix.[13] In Figure 2b, $\Sigma\mu_{1D}$ was plotted as a function of TPA content, where it clearly indicates an obvious drop at the TPA content of 50–70%. The $\Sigma\mu_{1D}$ values of the homopolymers (FL_{100} and TPA_{100}) are 0.7–0.8 cm^2 V^{-1} s^{-1}, revealing the high intramolecular charge carrier mobility.

2. 3. 3. DFT calculation of PTA-FL model tetramers

To account for the $\Sigma\mu_{1D}$ dependence on TPA content, density functional theory (DFT) calculations were carried out on the model tetramers after the geometry optimization using B3LYP/6-31G(d,p). The left column of Figure 3 illustrates the highest occupied molecular orbital (HOMO) of neutral states of the oligomers. The homopolymers (FL_{100} and TPA_{100}) as shown in Figure 3a and 3e demonstrate delocalized HOMO along the chain, which is consistent with their high intramolecular charge carrier mobilities observed by FP-TRMC. The delocalization is also observed in the singly occupied molecular orbital (SOMO) of the radical cations depicted in the right column of Figure 3. The planarization of the dihedral angle between each FL unit (from 36.5 to 29.3°) facilitates the molecular orbital delocalization in the radical cation as reported previously.[13, 18] In contrast, once the TPA unit is incorporated into the FL chains, the

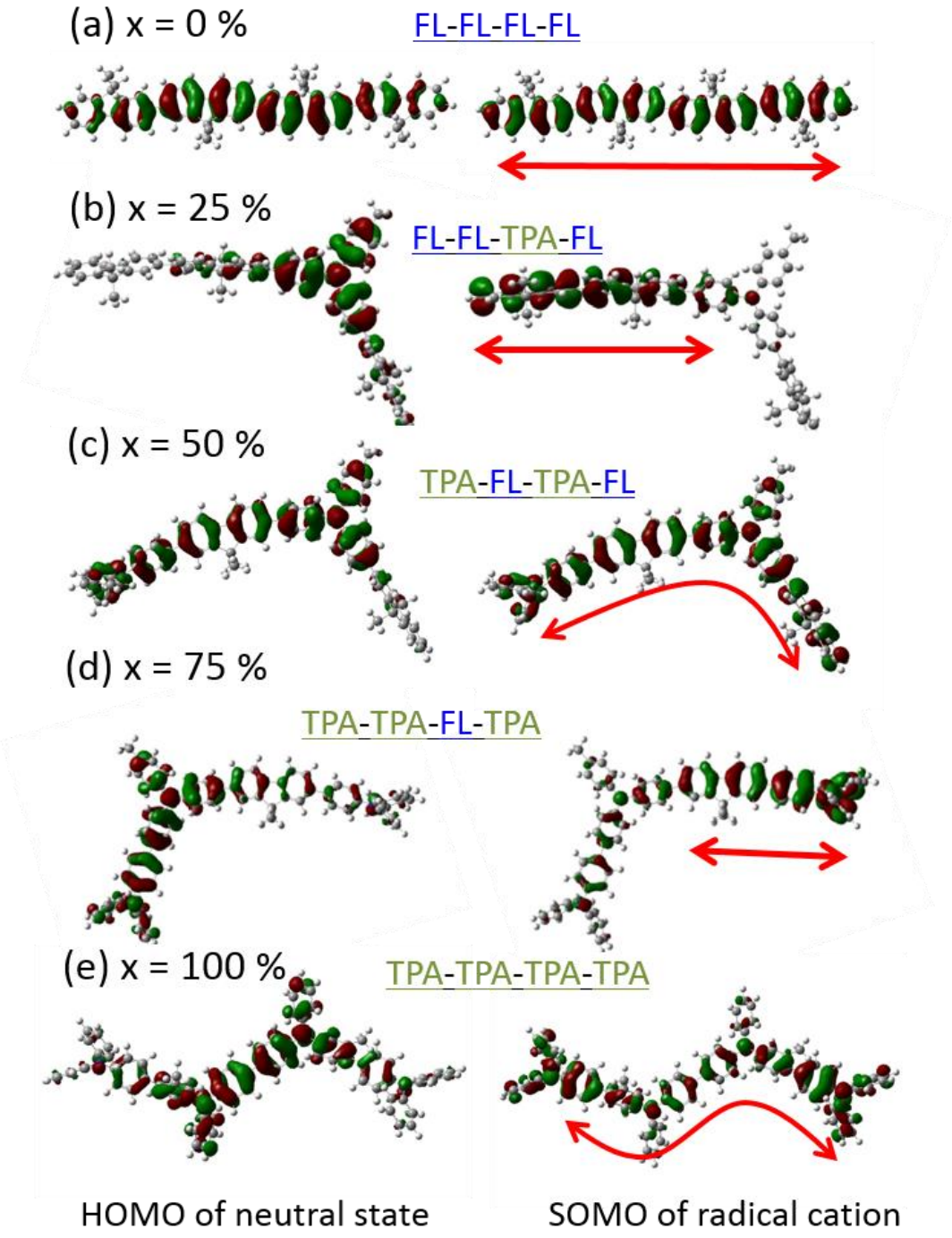

Figure 3. HOMO of neutral state (left) and SOMO of radical cation (right) of TPA–FL copolymers calculated by DFT using B3LYP/6-31G(d,p) function. The red arrows schematize the charge carrier motion probed by FP-TRMC.

electron-density states of HOMO and SOMO are altered. In the case of the FL–FL–TPA–FL tetramer displayed in Figure 3b, the HOMO of the neutral state is localized at the TPA unit; however, the SOMO is on the FL dimer units. Therefore, the intramolecular charge mobility in FL–FL–TPA–FL at TPA content = 25% should reflect the transport property of FL oligomer units. As seen in Figure 2b, $\Sigma\mu_{1D}$ values of $TPA_{10}FL_{90}$ and $TPA_{30}FL_{70}$ are almost comparable to that of FL_{100}, in good agreement with the previous report on fluorene–oligothiophene copolymers.[13] At the TPA content = 50% where the TPA and FL units are connected in alternating fashion, $\Sigma\mu_{1D}$ was decreased by about half of that of FL_{100}. As shown in Figure 3c, the HOMO of neutral TPA–FL–TPA–FL is centered at one FL unit and enclosed by two neighboring TPA units, while its SOMO of radical cation is extended to the other FL unit and delocalized over the whole tetramer. This is the case giving the high $\Sigma\mu_{1D}$; however, it was rather decreased in the FP-TRMC experiment. This contradiction is rationalized by considering the conformation of $TPA_{50}FL_{50}$ as an analogy to the fluorene-thiophene copolymers exhibiting an odd-even effect of thiophene units on the mobility.[13] Since the TPA has a large relative bond angle (ca. 120°) at the linkage, the conformation of the resultant $TPA_{50}FL_{50}$ polymer is in a zigzag form rather than straightforward like FL_{100}. This chain conformation leads to the decrease in $\Sigma\mu_{1D}$ probed by FP-TRMC, as it probes the charge carrier motion along the direction parallel to the microwave electric field in a resonant cavity. At the TPA content = 75% shown in Figure 3d, although the HOMO is localized on the TPA–TPA dimer part, the SOMO is mainly localized on one FL unit. Consequently, the hole on the FL unit isolated by TPA units cannot migrate effectively along the chain. Due to the zigzag conformation and charge confinement, $\Sigma\mu_{1D}$ became minimum at the TPA content = 75%. One presumption is that

the horizontal component of the SOMO delocalization correlates with the degree of intramolecular charge carrier motion probed by FP-TRMC.

2. 3. 4. SCLC and FET Measurement of PTA-FL Copolymers

Next, SCLC and FET measurements was performed to reveal the long-range intermolecular charge carrier mobilities. Hole-only SCLC [glass/indium tin oxide/poly(3,4-ethylenedioxythiophene):poly(styrene sulfonate)/copolymer/Au] and FET (channel length = 20 μm, channel width = 3 mm, cleaned SiO_2/n-doped Si, top-contact bottom-gate Au) devices were fabricated in accordance with a previous report. [19] Surprisingly, SCLC hole mobilities ($\mu_{h,SCLC}$) shown in Figure 4 indicate almost the same trend with FP-TRMC mobilities, though the former are more than six orders smaller (10^{-8} to 10^{-6} cm^2 V^{-1} s^{-1}) than the latter. In sharp contrast, FET hole mobilities ($\mu_{h,FET}$) exhibited a different dependence on the TPA content. The $\mu_{h,FET}$ revealed the lowest value for $TPA_{10}FL_{90}$ (9.8×10^{-7} cm^2 V^{-1} s^{-1}) and the highest value for $TPA_{50}FL_{50}$ (4.5×10^{-5} cm^2 V^{-1} s^{-1}). After reaching the maximum at TPA = 50%, $\mu_{h,FET}$ decrease simply with the TPA content. Although these mobilities are four to seven orders of magnitude smaller than those of FP-TRMC, it is interesting to find the same trend of FP-TRMC with SCLC and opposite one with FET. Pai et al. have reported the effect of the TPD molecule blended in poly(N-vinylcarbazole) (PVCz) matrix on the time-of-flight (TOF) hole mobilities.[20] They have shown that the mobility was minimized in the presence of a small concentration of TPD (ca. 2wt %), because the TPD molecule, the ionization potential of which is smaller than that of carbazole, acts as a trap for charge transport. Further increasing TPD concentration improved the mobility and sooner it became superior to pristine PVCz, once the hopping distance among TPD was shortened by

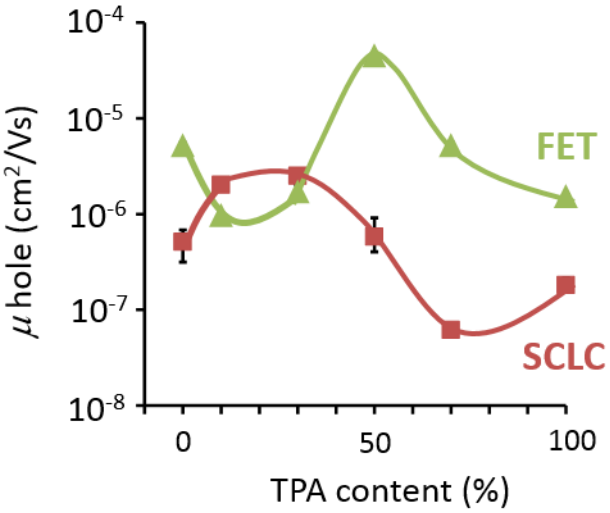

Figure 4. (a) Hole mobilities estimated by SCLC (red squares) and FET (green triangles) as a function of TPA content.

incorporating a large amount of TPD. The dependence of $\mu_{h,FET}$ of TPA–FL copolymers on the TPA content from 0 to 50% is analogous to that reported in the TPD–PVCz system. On the other hand, the decrease of $\mu_{h,FET}$ found for $TPA_{70}FL_{30}$ and TPA_{100} is probably due to the restriction of optimal intermolecular π-orbital overlap of the TPA units involved in the copolymer backbone. This decrease of mobility at the high TPA concentration is a sharp contrast to that observed in TPD molecular glasses, where the molecular TPD can easily reorganize their configurations in the film states to maximize the transfer integral. [21, 22] Our interest is focused on the reason why $\mu_{h,SCLC}$ and FP-TRMC mobility indicated the similar dependence on the TPA content, although they are completely different measurements, direct current (dc) and alternating current (ac), respectively. The charge carrier densities and applied electric field of FET and SCLC techniques are around 10^{19} cm^{-3} and 10^5 Vcm^{-1}, respectively, while those of FP-TRMC are on the order of ca. 10^{16} cm^{-3} and 100 Vcm^{-1}. The lengths of charge transport of FP-TRMC, SCLC, and FET are a few nanometers, [23] 100–200 nm, and 20 μm, respectively. Therefore, the similarity

between FP-TRMC and SCLC in comparison with FET is the relatively close transport length. FET devices with longer channel length (50 μm) was examined preliminarily and found that the mobility was decreased by 30–50%. Much longer channel devices (> 100 μm) failed to operate, implying that $\mu_{h,FET}$ has a negative dependence on the channel length. These results suggest that intramolecular charge properties such as SOMO delocalization and polymer conformation are more predominant in the short-range charge transport for both ac and dc measurements. Another similarity between SCLC and FP-TRMC is that they probe bulk mobility, while the charge carriers in FET device are transported in a monomolecular layer at dielectric/semiconductor interface. Lucas et al. investigated SCLC, FET, and impedance spectroscopy of pentacene films and suggested the observed difference in their mobilities arose from active layer morphology for different substrate and electric/electronic processes involved in the measurements. [24] Further investigation is highly anticipated to clarify the distance, carrier density, and frequency dependences on the charge carrier mobility, along with the effects of film thickness, surface morphology, and grain size. In particular, choice of gate insulator[25] or surface treatment[26] is a critical factor for FET mobilities.

2. 4. Conclusion

In conclusion, SCLC and FP-TRMC mobilities demonstrated a similar trend on the TPA contents of TPA–FL copolymers with the minimum mobility at the TPA content = 70%. The short-range mobilities on a few nanometer scales revealed by FP-TRMC, reflecting mainly the intramolecular charge transport, are rationalized by the SOMO delocalization of the radical cation and the conformation of the polymer backbone. In contrast, the FET mobility indicated the almost opposite dependence on the TPA content, showing the minimum at the TPA content = 10%. The FET results are coincident with the TOF experiments reported in TPD–PVCz blend films, where a small amount of TPD acts as a trap. The present study elucidated the interplay of TPA content for intra- and intermolecular charge carrier mobilities, thereby indicating the importance of distance-dependent charge carrier transport.

2. 5. References and notes

[1] Kim, J.-S.; Lu, L.; Sreearunothai, P.; Seeley, A.; Yim, K.-H.; Petrozza, A.; Murphy, C. E.; Beljonne, D.; Cornil, J.; Friend, R. H. *J. Am. Chem. Soc.* **2008**, *130*, 13120.

[2] Zhang, W.; Smith, J.; Hamilton, R.; Heeney, M.; Kirkpatrick, J.; Song, K.; Watkins, S. E.; Anthopoulos, T.; McCulloch, I. *J. Am. Chem. Soc.* **2009**, *131*, 10814–10815.

[3] Su, W.-F.; Chen, Y.; *Polymer* **2011**, *52*, 77.

[4] Pasini, M.; Giovanella, U.; Betti, P.; Bolognesi, A.; Botta, C.; Destri, S.; Porzio, W.; Vercelli, B.; Zotti, G. *ChemPhysChem* **2009**, *10*, 2143−2149.

[5] Zhang, Z.; Zhang, K.; Liu, G.; Zhu, C.; Neoh, K. G.; Kang, E. T. *Macromolecules* **2009**, *42*, 3104.

[6] Shen, P.; Tang, Y.; Jiang, S.; Chen, H.; Zheng, X.; Wang, X.; Zhao, B.; Tan, S. *Org. Electron.* **2011**, *12*, 125.

[7] Nakata, M.; Kawano, K.; Yasumatsu, M.; Yahiro, M.; Adachi, C. *Appl. Phys. Express* **2010**, *12*, 125.

[8] Pihosh, Y.; Turkevych, I.; Goto, M.; Kasahara, A.; Takamasu, T.; Tosa, M. *Jpn. J. Appl. Phys.* **2008**, *47*, 1263.

[9] Oka, N.; Kato, K.; Yagi, T.; Taketoshi, N.; Baba, T.; Ito, N.; Shigesato, Y. *Jpn. J. Appl. Phys.* **2010**, *49*, 121602.

[10] Chun, M.-S.; Teraji, T.; Ito, T. *Jpn. J. Appl. Phys.* **2003**, *42*, 5233.

[11] Satoh, N.; Cho, J. S.; Higuchi, M.; Yamamoto, K. *J. Am. Chem. Soc.* **2003**, *125*, 8104.

[12] Saeki, A.; Seki, S.; Satoh, N.; Yamamoto, K.; Tagawa, S. *J. Phys. Chem. B* **2008**, *112*, 15540.

[13] Saeki, A.; Fukumatsu, T.; Seki, S. *Macromolecules* **2011**, *44*, 3416.

[14] Saeki, A.; Tsuji, M.; Seki, S. *Adv. Energy Mater.* **2011**, *1*, 661.

[15] Yasuda, T.; Yamaguchi, Y.; Zou, D.-C.; Tsutsui, T.; *Jpn. J. Appl. Phys.* **2002**, *41*, 5626.

[16] Xin, H.; Ren, G.; Kim, F. S.; Jenekhe, S. A. *Chem. Mater.* **2008**, *20*, 6199.

[17] Blom, P. W. M.; deJong, M. J. M.; Vleggaar, J. J. M. *Appl. Phys. Lett.* **1996**, *68* 3308.

[18] Fratiloiu, S.; Grozerna, F. C.; Koizumi, Y.; Seki, S.; Saeki, A.; Tagawa, S.; Dudek, S. P.; Siebbeles, L. D. A. *J. Phys. Chem. B* **2006**, *110*, 5984.

[19] Balan, B.; Vijayakumar, C.; Saeki, A.; Koizumi, Y.; Seki, S. *Macromolecules* **2012**, *45*, 2709.

[20] Pai, D. M.; Yanus, J. F.; Stolka, M. *J. Phys. Chem.* **1984**, *88*, 4714.

[21] Marcus, R. A. *J. Chem. Phys.* **1956**, *24*, 966.

[22] Yamada, T.; Sato, T.; Tanaka, K.; Kaji, H. *Org. Electron.* **2010**, *11*, 255.

[23] Saeki, A.; Yamamoto, Y.; Koizumi, Y.; Fukushima, T.; Aida, T.; Seki, S. *J. Phys. Chem. Lett.* **2011**, *2*, 2549.

[24] Lucas, B.; El Amrani, A.; Moliton, A.; Skaiky, A.; El Hajj, A.; Aldissi, M. *Solid-State Electron.* **2012**, *69*, 99.

[25] Uemura, T.; Yamagishi, M.; Ono, S.; Takeya, J. *Jpn. J. Appl. Phys.* **2010**, *49*, 01AB13.

[26] Umeda, T.; Kumaki, D.; Tokito, S. *J. Appl. Phys.* **2009**, *105*, 024516.

Chapter 3

Separation of Intra- and Inter-Molecular Charge Carrier Mobilities of Poly(3-hexylthiophene) in Insulating Polystyrene Matrix

3. 1. Abstract

Optoelectronic and optical properties of poly(3-hexylthiophene-2,5-diyl) (P3HT) diluted in polystyrene (PS) matrices were investigated by flash-photolysis time-resolved microwave conductivity (FP-TRMC) and steady-state photoabsorption spectroscopy, respectively. Intra- and inter-molecular charge carrier mobilities in the blend and pristine P3HT films was examined. It was revealed the contribution of *inter*-molecular charge carrier mobility is half at the maximum in the pristine film. This in turn gave information about the minimum one-dimensional *intra*-molecular mobility of 0.18 cm^2/Vs.

3. 2. Introduction

In recent years, organic electronic devices such as organic field effect transistor (OFET) and organic photovoltaic cells (OPV), have been rapidly developed, and conjugated polymers with high charge carrier mobility have received considerable attention because of flexibility, lightweight, facile tuning of optical and electrical properties via molecular design, and so on.[1] Charge carrier mobility, especially intermolecular charge carrier mobility, is one of the most important factors for high-performance devices of OFET and OPV. On the contrary, intramolecular mobility is expected to be higher than intermolecular one due to extent of conjugation along the main chain. However, the direct observation of intramolecular charge carrier mobility has been difficult by conventional electric measurements.

For the removal of the contribution from intermolecular charge carrier mobility, a convenient and effective way is that conjugated polymers are dispersed into an insulating matrix to reduce intermolecular interactions, as illustrated in Figure 1. However, it is difficult to measure the electrical conductivity of isolated conjugated polymer in the insulating matrix by using electrode-contact methods like field-effect transistor (FET) and/or time-of-flight (TOF). Instead, flash-photolysis time-resolved microwave

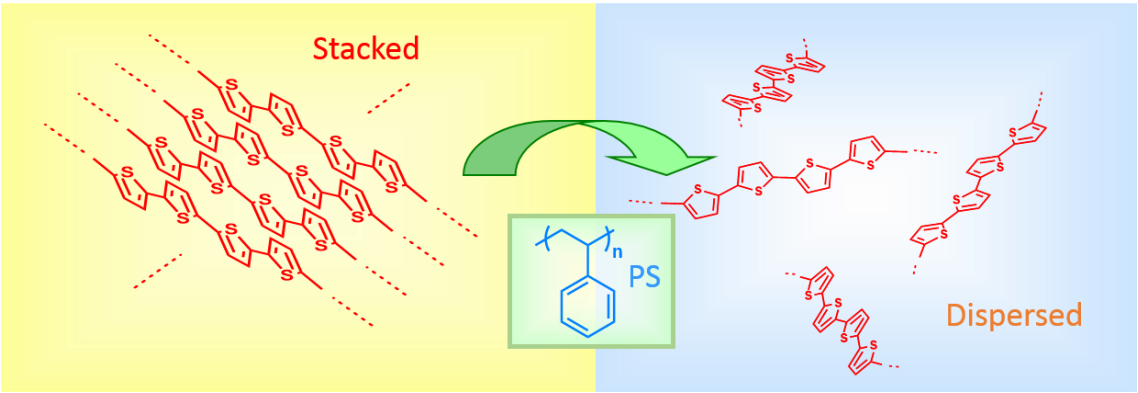

Figure 1. Illustration of stacked P3HT and dispersed P3HT in PS.

conductivity measurement (FP-TRMC),[2, 3] one of the alternating current measurements, can be employed as an effective way of conductivity measurement in such an insulation matrix, because it can probe the oscillational motion of charge carrier under electromagnetic wave without contacting the semiconductors.

In this work, a typical p-type conjugated polymer of regio-regular poly(3-hexylthiophene-2,5-diyl): P3HT in polystyrene (PS) matrix was investigated using FP-TRMC and steady-state photoabsorption spectroscopy.

3. 3. Experimental Section

P3HT (weight-averaged molecular weight: $M_w = 1.0 \times 10^5$) and PS ($M_w = 2.8 \times 10^5$) were purchased from Aldrich and used without further purification. Transient photoconductivity was performed by FP-TRMC system. The detail of the system is reported in the literature.[2] A Nd:YAG laser (355 nm) (Spectra-Physics) with 4.6×10^{15} photons/cm^2 was used as excitation source. All the experiments were performed under an ambient condition.

The blend films of PS and P3HT were prepared by drop-casting on a quartz plate from chlorobenzene solutions. The blend ratio was ranging from 0.05 to 20 wt % relative to 100 wt% PS and controlled by mixing the corresponding fraction of the original P3HT solution (0.1 wt%) and PS solution (10 wt%). The films were dried in a vacuum oven at 60 ˚C. Electronic absorption spectroscopy was performed using a JASCO model V-570.

3. 4. Result and Discussion

3. 4. 1. Electronic absorption of P3HT+PS films

In order to investigate the P3HT conformation in PS, electronic absorption spectra were investigated for P3HT+PS films ranging contents of P3HT from 0.05 to 20 wt% . As shown in Figure 2, the absorption maxima are abruptly shifted from 520 to 550 nm from P3HT : PS = 0.5 : 100 to 1 : 100. Simultaneously the absorption shoulders at around 600 nm are gradually grown. This shoulder is understood as a π-stack and/or planarization of polythiophene backbone. The solvatochromism and thermochromism of regio-regular and regio-random polythiophenes were well documented in terms of the main chain conformation.[4] It should be noted that regio-regular and regio-random polythiophenes (PT) showed almost identical absorption spectra in a good solvent like chloroform and chlorobenzene; however, the absorption peak of regio-regular PT in vibronic peak

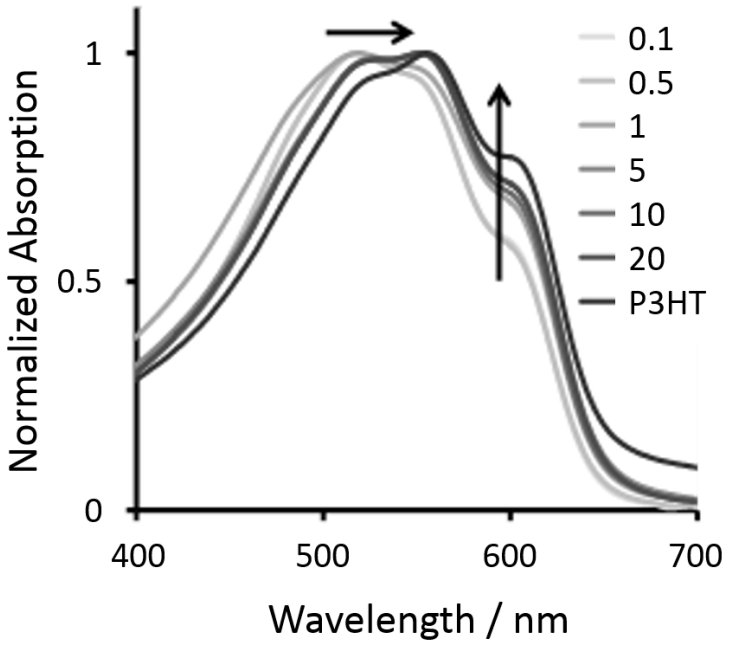

Figure 2. Electronic transition spectra of P3HT+PS blend films. The blend ratios of P3HT:PS are 0.1-20: 100 (wt%). The black solid line (P3HT) is a pristine film without PS. The arrows indicate the increase of P3HT content in the mixture.

appears at ca. 600 nm and a clear diffraction peaks were observable by X-ray diffraction measurement.[3] Recently, self-threading polythiophene (ST-PT) molecular wire covered by insulating alkyl chains has been synthesized, where the dihedral angle of neighboring two thiophenes are planarized by the alkyl insulators.[5] Interestingly, this ST-PT with rigid backbone shows vibronic shoulder even in a solution. These results are suggestive that the shoulder is due to the planarization and extension of persistent length of isolated polythiophene backbone, which leads to the strong intermolecular π-stacking and the formation of crystalline lamellar domain in the film state. Actually, the planarization of polymer and π-stacking occurs cooperatively during the transition from solution to film state.

The electronic absorption spectra of P3HT+PS films shown in Figure 2 have the shoulder even at the lowest P3HT concentration, indicating that the polymer is planarized in PS matrix. Although both P3HT and PS possess hydrophobic nature, the small difference of surface energy (20 and 26 mJ/m^2, respectively) has been reported to promote phase separation at high P3HT content.[6] The abrupt shift of absorption maxima mentioned in the previous paragraph might be the signature of the phase separation and resultant increase of intermolecular π-stack and further planarization. Note that extreme phase separation was observed for the mixture of P3HT and hydrophilic polymer such as poly(methyl methacrylate): PMMA with the surface energy of 44 mJ/m^2.[6]

FP-TRMC measurements were performed for the P3HT+PS blend films using 355 nm as an excitation wavelength. At this wavelength, only P3HT absorbs the light source, forming excited states of P3HT. They dissociate into positive and negative charges within the time resolution of FP-TRMC system. The transient photoconductivity was converted to a $\phi\Sigma\mu$ value, which is a product of ϕ (quantum efficiency of charge carrier generation)

and $\Sigma\mu$ (sum of mobilities of positive and negative charge carriers).

Figure 3 shows the maximum $\phi\Sigma\mu$ value ($\phi\Sigma\mu_{max}$) of each transient plotted as a function of P3HT concentration. The effect of increasing steady-state photoabsorptions of the blend films with the P3HT concentration is compensated in the $\phi\Sigma\mu$ representation. For the films prepared by one-time drop-casting (open circles), $\phi\Sigma\mu_{max}$ at low P3HT content (0.05 – 1 : 100) indicates the almost constant value of 1×10^{-4} cm^2/Vs; however, it turns to increase up to 1.5×10^{-4} cm^2/Vs at P3HT : PS = 20 : 100. It is noteworthy that this change is coincident with the sudden shift of the photoabsorption maximum of the blend film in Figure 2, suggesting that *inter*-molecular transient conductivity of P3HT correlates directly with the backbone configuration of steady- and radical ionic states of the molecules.

More interestingly, the thicker films prepared by two-time drop-casting (closed triangles) show a considerable increase of $\phi\Sigma\mu_{max}$ even at low P3HT content. During the second drop-casting, the initial thin film was dissolved again in the second droplet, giving highly-concentrated P3HT+PS solution on the quartz plate. Therefore intermolecular π-stacking of P3HT occurs more efficiently in the thick films during the solvent evaporation. This is the case giving the dramatic increase of $\phi\Sigma\mu_{max}$ even at low P3HT content. Even for the thin films predominant at more than 1 wt% P3HT, as shown in Figure 3. Thus, It was predict that P3HT molecules in the *thin* films of P3HT : PS = 0.05 – 1 : 100 are dispersed and isolated in the PS matrix.

The $\phi\Sigma\mu_{max}$ of pristine P3HT film ranges from 2 to 5×10^{-4} cm^2/Vs, depending on the solvent, concentration, and thermal annealing. Based on the same condition with the present study, the bare P3HT film showed $\phi\Sigma\mu_{max}$ of 2×10^{-4} cm^2/Vs, which was twice of the abovementioned isolated P3HT molecules in the PS matrix.[3] In the π-stacked

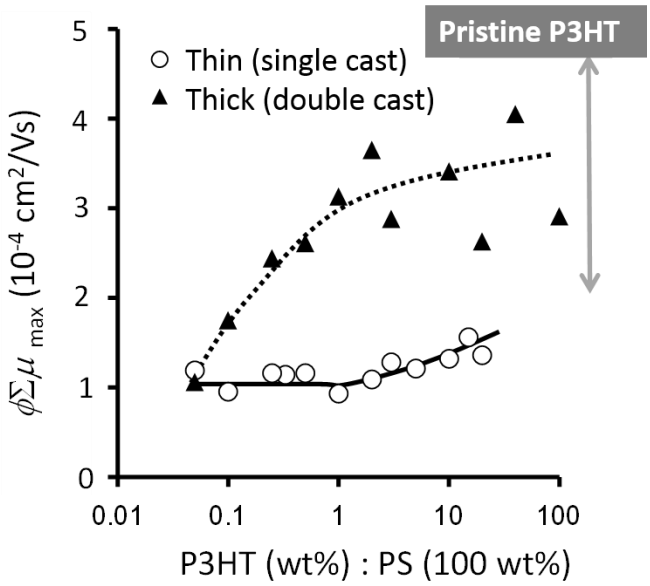

Figure 3. $\phi\Sigma\mu_{max}$ vs P3HT mixing ratio in P3HT+PS blend films measured by FP-TRMC excited at 355 nm. The open circles and closed triangles are the films prepared by single and double drop-casting, respectively. The gray arrow labeled by "Pristine P3HT" represent the range of $\phi\Sigma\mu_{max}$ of pure P3HT film. The value is significantly dependent on the process condition.

lamellar domain of P3HT, intermolecular excitons were generated more preferably than in amorphous phase, and thus the charge carrier generation efficiency (ϕ) was enhanced.[7] Therefore some portions of the increase of $\phi\Sigma\mu_{max}$ found in the pristine P3HT film might be attributed to the increase of ϕ. This in turn implies that the contribution of *inter*-molecular charge carrier mobility to the $\Sigma\mu$ value is half at the maximum.

$\Sigma\mu$ value of P3HT bulk film has been estimated by FP-TRMC using a perylenebisimide derivative as an electron acceptor and spectroscopic probe. The value was 0.12 cm^2/Vs.[3] Consequently, three-dimensional *intra*-molecular charge carrier mobility of P3HT dispersed in the PS matrix is more than 0.06 cm^2/Vs. Supposed that the orientation of P3HT molecule in the matrix is random (probably true), one-dimensional *intra*-molecular charge carrier mobility along the P3HT chain is expected to be more than 0.18 cm2/Vs, since the observed mobility is one-third of the one-dimensional value. This value is higher

than the *highest* FET mobility reported in the P3HT films (0.1 cm^2/Vs), while the typical FET mobilities of P3HT films are usually lying in much lower orders of 10^{-3} to 10^{-4} cm^2/Vs.[8] This is suggestive that planarization of P3HT molecule from solution to film states improves both intra- and inter-molecular charge carrier mobilities, where the latter is secured by the strong π-stacking of the planar polymer backbone.

3. 5. Conclusion

Transient photoconductivities of P3HT+PS blend films were investigated by FP-TRMC. $\phi\Sigma\mu_{max}$ values of the thin films at low P3HT content (0.05 - 1) were almost constant and dominated mainly by *intra*-molecular charge carrier mobility of isolated P3HT molecule. The increase of $\phi\Sigma\mu_{max}$ with P3HT content is consistent with the steady-state photoabsorption spectra. The *minimum* one-dimensional mobility was estimated as 0.18 cm^2/Vs and the contribution of *inter*-molecular charge carrier mobility to the $\phi\Sigma\mu_{max}$ of pristine P3HT film is half at the maximum. We expect that intra-molecular charge carrier mobility is still higher than 0.18 cm^2/Vs, which could be revealed by developing a novel matrix specific to FP-TRMC measurement.

3. 6. References and Notes

[1] (a) Skotheim, T. A.; Elsenbaumer, R. L.; and Reynolds, J. R. In *Handbook of Conducting Polymer,* Marcel Dekker, New York, 1998. (b) McCullough, R. D.; Tristram-Nagle. S.; Williams, S. P.; Lowe, R. D.; Jayaraman, M. *J. Am. Chem. Soc.* **1993**, *115*, 4910. (c) Chen, T.-A.; Rieke, R. D. *J. Am. Chem. Soc.* **1992**, *114*, 10087. (d) Yamamoto, T.; Arai, M.; Kokubo, H.; Sasaki, S. *Macromolecules* **2003**, *36*, 7986.

[2] (a) Saeki, A.; Yamamoto, Y,; Koizumi, Y.; Fukushima, T.; Aida, T.; Seki, S. *J. Phys.*

Chem. Lett. **2011**, *2*, 2549. (b) Saeki, A.; Tsuji, M.; Seki, S. *Adv. Energy Mater.* **2011**, *1*, 661. (c) Saeki, A.; Fukumatsu, T.; Seki, S. *Macromolecules* **2011**, *44*, 3416. (d) Zhang, W.; Jin, W.; Fukushima, T.; Saeki, A.; Seki, S.; Aida, T. *Science* **2011**, *334*, 340. (e) Saeki, A.; Seki, S.; Takenobu, T.; Iwasa, Y.; Tagawa, S. *Adv. Mater.* **2008**, *20*, 920. (f) Warman, J. M.; Gelinck, G. H.; de Haas, M. P. *J. Phys.: Condens. Matter* **2002**, *14*, 9935. (g) Grozema, F. C.; Siebbeles, L. D. A.; Warman, J. M.; Seki, S.; Tagawa, S.; Scherf, U. *Adv. Mater.* **2002**, *14*, 228. (h) Prins, P.; Grozema, F. C.; Schins, J. M.; Patil, S.; Scherf, U.; Siebbeles, L. D. A. *Phys. Rev. Lett.* **2006**, *96*, 146601.

[3] (a) Saeki, A.; Ohsaki, S.; Seki, S.; Tagawa, S. *J. Phys. Chem. C* **2008**, *112*, 16643. (b) Saeki, A.; Ohsaki, S.; Koizumi, Y.; Seki, S.; Tagawa, S. *Synth. Met.* ***2009***, *159*, 1800. (c) Saeki, A.; Ohsaki, S.; Koizumi, Y.; Seki, S.; Tagawa, S. *J. Photopolym. Sci. Technol.* **2008**, *21*, 559.

[4] Leclerc, M.; Faid, K.; *Adv. Mater.* **1997**, *14*, 1087.

[5] Sugiyasu, K.; Honsho, Y.; Harrison, R. M.; Sato,; A. Yasuda, T.; Seki, S.; Takeuchi, M. *J. Am. Chem. Soc.* **2010**, *132*, 14754.

[6] Honda, S.; Ohkita, H.; Benten, H.; Ito, S. *Adv. Energy Mater.* **2011**, *1*, 588.

[7] (a) Jiang, X. M.; Österbacka, R.; Korovyanko, O.; An, C. P.; Horovitz, B.; Janssen, R. A. J.; Vardeny, Z. V. *Adv. Funct. Mater.* **2002**, *12*, 587. (b) Guo, J.; Ohkita, H.; Benten, H.; Ito, S. *J. Am. Chem. Soc.* **2010**, *132*, 6154.

[8] (a) Sirringhaus, H.; Brown, P. J.; Friend, R. H.; Nielsen, M. M.; Bechgaard, K.; Langeveld-Voss, B. M. W.; Spiering, A. J. H.; Janssen, R. A. J.; Meijer, E. W. Herwing, P.; de Leeuw, D. M. *Nature* **1999**, *401*, 685. (b) Sirringhaus, H.; Tessler, N.; Friend, R. H. *Science* **1998**, *280*, 1741. (c) Ong, B. S.; Wu, Y.; Liu, P.; Gardner, S. *J. Am. Chem. Soc.* **2004**, *126*, 3378.

General Conclusion

In this thesis, the author studied the impact on the charge transport property of conjugated polymer given by the change of secondary structure by FP-TRMC. The new findings in this thesis are summarized as follows.

Chapter 1

The intramolecular charge carrier mobilities in fluorene-thiophene copolymers (pFTn-x%) were investigated by FP-TRMC measurement. In the copolymers of x = 50% and 20%, odd-even effect was shown for the number of oligothiophene units, and the odd-numbered copolymers had lower intramolecular charge carrier mobility than the even-numberd ones. On the other hund, in the 10% and 2% copolymers no odd-even effect was shown and the mobility converged to ca. 0.7 cm^2 V^{-1} s^{-1}, which was equal to that of polyfluorene. This odd-even effect was ascribed to the zigzag configuration of the main chain by the rotation of the fluorene units due to the interaction of alkyl chains and solvent used in film priparation. It was implied that FP-TRMC measurement can detect the intramolecular charge carrier mobility of amorphous polymers reflected the polymer configuration.

Chapter 2

The charge transport property of TPA–FL copolymers was evaluated by FP-TRMC technique. The intramolecular charge carrier mobilities depended on TPA contents of TPA–FL copolymers, and minimum mobility was evaluated at the TPA content = 70% copolymer. By DFT calculation, this decrease was ascribed to the zigzag formation of the polymer backbone and the localization of SOMO, and it was implied that the short-range mobilities on a few nanometer scale reflected mainly the intramolecular charge transport

would be evaluated in FP-TRMC technique. Furthermore, SCLC and FET measurement were performed, and the FP-TRMC mobility indicated almost the opposite dependence on the TPA content to the FET mobility. This result revealed that the intramolecular charge carrier mobility reflected polymer backbone structure can be evaluated in FP-TRMC technique, while FET mobility shows the long-distance charge carrier transport

Chapter 3

By polymer alloy technique, the charge carrier mobility of P3HT in PS matrix was investigated by FP-TRMC-technique. It was revealed that in low P3HT concentration the contribution of *inter*-molecular charge carrier mobility of P3HT is more decreased than pristine P3HT film. It was implied that the charge carrier mobility 0.18 cm^2/Vs of PS+P3HT polymer alloy evaluated by FP-TRMC technique showed the intramolecular charge transport property.

Throughout this thesis, the author studied the correlation between the secondary structure of the polymer backbone and the charge carrier mobility. It is revealed that linear polymer backbone is the advantage for the intramolecular charge transport and the backbone structure have strong influence for the charge transport as well as the delocalization of the electron on the polymer chain. Furthermore, polymer alloy technique can be applied for the methods to evaluate the correlation between the charge carrier mobility and the backbone structure. Because this technique can be applicable to various conductive polymers, it can be revealed that how secondary structure is better for charge transport property.

The author wishes to lead these studies to the criteria for conjugated polymers with backbone structure which is the best for charge transport.

Acknowledgement

The study in present thesis is the summary of from 2010 to 2015 at the Division of Applied Chemistry, Graduate School of Engineering, Osaka University under the supervision of Professor Shuhei Seki.

The author would like to express his deepest gratitude to Professor Shuhei Seki for his precise suggestion and helpful discussion, hearty encouragement to the author. The author also deeply indebted to Associate Professor Akinori Saeki for his stimulating suggestion, informative discussion and untiring patience.

The author also wish to thanks the members of Seki's laboratory, Professor Motohiro Nakano, Dr. Kazuyuki Enomoto, Ms. Yuko Fujiie, Professor Tsuneaki Sakurai, Dr. Daisuke Sakamaki, Dr. Masaaki Omichi, Dr. Naoto Matsuyama, Dr. Yoshiko Koizumi, Dr. Wakana Matsuda, Dr. Haruyuki Baba, Dr. Yoshihito Honsho, Ms. Shima Nakanishi, Dr. Atsushi Asano, Mr. Sohei Enomoto, Mr. Tsubasa Mikie, Mr. Yuta Maeyoshi, Mr. Kenji Kuwada, Mr. Masashi Tsuji, Mr. Takenori Fujiwara, Mr. Yoshihiro Yasutani, Ms. Hiromi Marui, Mr. Sho Yamanaka, Ms. Marina Ide, Ms. Tomoyo Miyakai, Ms. Saya Yoshikawa, Mr. Yuki Takeshita, Mr. Satoru Yoneda, Mr. Yuki Noguchi, Mr. Wook Jin Choi, Mr. Yoshihiro Shioaku. Ms. Mariko Noguchi, Ms. Eman Al-Naamani, Mr. Toshiyuki Kobashi, Mr. Yusuke Tsutsui, Mr. Hikaru Oga, Mr. Masataka Kumano, Mr. Naoki Ishida, Mr.Yoshiki Shimata, Mr. Yuki Tsujimoto, Mr. Hiroshi Tomita, Mr. Akihumi Horio, and Mr. Tuchinda Wasin.

The author is grateful to the Research Fellowships of the Japan Society for the Promotion of Science for Young Scientists for financial support.

Finally, the author would like to express his thanks to his parents, Hirohito Fukumatsu

and Mayumi Fukumatsu, his sisters, Saori Fukumatsu, Aya Fukumatsu, and grandmother Kikue Fukumatsu for their contiuous support, understanding, and encouragement.

List of Publication

1. Saeki, A.;Fukumatsu, T.; Seki, S.

   Intramolecular Charge Carrier Mobility in Fluorene-Thiophene Copolymer Films Studied by Microwave Conductivity

   Macromolecules **2011**, *44*, 3416.

2. Fukumatsu, T.;S aeki, A.; Seki, S.

   Charge Carrier Mobilities in Amorphous Triphenylamine–Fluorene Copolymers: Role of Triphenylamine Unit in Intra- and Intermolecular Charge Transport

   Appl. Phys. Express **2012**, *5*, 061701.

3. Fukumatsu, T.; Saeki, A.; Seki, S.

   Separation of Intra- and Inter-Molecular Charge Carrier Mobilities of Poly(3-hexylthiophene) in Insulating Polystyrene Matrix

   J. Photopolym. Sci. Technol. **2012**, *25*, 665.

Supplementary Publication

1. Seki, S.; Fukumatsu, T.; Saeki, A..

   Intra-Molecular Mobility of Charge Carriers along Conjugative Macromolecular Backbones

   Kobunshi Ronbunshu **2011**, *68*, 53.

2. Yasutani, Y.; Saeki, A.; Fukumatsu, T.; Koizumi, Y.; Seki, S.

   Unprecedented High Local Charge-Carrier Mobility in P3HT Revealed by Direct and Alternating Current Methods

   Chem. Lett. **2013**, *42*, 19.

3. Wang, H.; Fukumatsu, T.; Liu, Y.; Hu, W.; Seki, S.; Zhan, X.

   A–D–A–D Swivel-Cruciform Oligothiophene Based on 5,5’-bibenzothiadiazole

   J. Mater. Chem. C **2013**, *1*, 414.